Multiscale Modeling of Thermal and Electrical Characteristics in Silicon CMOS Devices

by

Robin Daugherty

A Dissertation Presented in Partial Fulfillment
of the Requirements for the Degree
Doctor of Philosophy

Approved November 2019 by the
Graduate Supervisory Committee:

Dragica Vasileska, Chair
James Aberle
David Ferry
Stephen Goodnick

ARIZONA STATE UNIVERSITY

December 2019

ABSTRACT

This dissertation explores thermal effects and electrical characteristics in metal-oxide-semiconductor field effect transistor (MOSFET) devices and circuits using a multiscale dual-carrier approach. Simulating electron and hole transport with carrier-phonon interactions for thermal transport allows for the study of complementary logic circuits with device level accuracy in electrical characteristics and thermal effects. The electrical model is comprised of an ensemble Monte Carlo solution to the Boltzmann Transport Equation coupled with an iterative solution to two-dimensional (2D) Poisson's equation. The thermal model solves the energy balance equations accounting for carrier-phonon and phonon-phonon interactions. Modeling of circuit behavior uses parametric iteration to ensure current and voltage continuity. This allows for modeling of device behavior, analyzing circuit performance, and understanding thermal effects.

The coupled electro-thermal approach, initially developed for individual n-channel MOSFET (NMOS) devices, now allows multiple devices in tandem providing a platform for better comparison with heater-sensor experiments. The latest electro-thermal solver allows simulation of multiple NMOS and p-channel MOSFET (PMOS) devices, providing a platform for the study of complementary MOSFET (CMOS) circuit behavior. Modeling PMOS devices necessitates the inclusion of hole transport and hole-phonon interactions. The analysis of CMOS circuits uses the electro-thermal device simulation methodology alongside parametric iteration to ensure current continuity. Simulating a CMOS inverter and analyzing the extracted voltage transfer characteristics verifies the efficacy of this methodology. This work demonstrates the effectiveness of the dual-carrier electro-thermal solver in simulating thermal effects in CMOS circuits.

DEDICATION

For my family

For my mom - Penny Daugherty - my mom has been the ultimate source of encouragement and support. Whatever I chose to pursue, she accepted my choice and insisted that I approach it with vigor and dedication. She taught me to take responsibility for my success and to find the lessons in my failures. Thanks mom!

For my dad - Peter Daugherty - if anyone can be credited with motivating me to pursue a PhD, it's my dad. I remember sitting in the study watching him work on his research, which happened to involve simulations of natural systems. By coincidence or providence, modeling of physical systems is at the core of my own research as well. Thanks dad!

For my brother - Brian Daugherty - we both take after our dad in pursuing a PhD, but Brian helped convinced me I should choose my own path. As a kid, I could never match my older brother's achievements if I only followed his lead. I learned to identify my own strengths and strive for my own accomplishments. Thanks Brian!

ACKNOWLEDGMENTS

I would not have been able to complete this dissertation without help from many individuals along the way. I would like to extend my thanks and show my gratitude for the professors, colleagues, and friends who helped me achieve this goal.

Dragica Vasileska, my dissertation advisor and chair of my defense committee, spent countless hours helping me with my project: discussing theory, debugging code, analyzing results, writing abstracts, practicing for conference talks, and of course preparing and defending this dissertation.

James Aberle is a member on my defense committee and the professor for whom I've worked as a teaching assistant during my graduate program. He allowed and encouraged me to take a proactive approach in my role as a TA: making lesson plans, scheduling meetings with students, planning assignments, etc. This helped me come into my own as an academic and gave me the confidence to solve problems on my own.

Virginia Klimeck, a close friend of Dr. Vasileska, provided immeasurable assistance in reviewing and revising this manuscript. Her expertise in grammar and technical writing helped ensure this dissertation is polished and exact.

Pradyumna Muralidharan, a colleague in Dr. Vasileska's research group, was at ASU when I started my PhD and has been a dear friend to me throughout. When Prado finished his PhD, I knew it was time for me as well.

Genevieve Hall, my loving partner, has shown me unending patience, care, and support.

TABLE OF CONTENTS

Page

LIST OF TABLES

Table Page

LIST OF FIGURES

Figure Page

Figure Page

CHAPTER 1

INTRODUCTION AND LITERATURE SURVEY

1.1 Introduction

Silicon based microelectronics has long been a driving force in computing, communications, and other areas of technology which drastically affect the way people interact with the world. From the earliest integrated circuits to the latest in novel device topologies and advanced architecture, many of the critical operating principles in microelectronic circuits and devices have not changed. One example is the ubiquitous use of complementary transistor pairings in analog and digital circuits [1]. The study of silicon-based microelectronics – both historically and in modern applications – includes carefully analyzing the operational principles of p-n junctions, MOSFETs and BJTs, as well as the design of advanced analog and digital circuits. The ubiquity of CMOS is clear in both analog and digital circuit design. Even as modern device structures deviate further in design and operating principle from traditional planar MOSFETs, it is likely that transistors with complementary conductivity type (as seen in the n- and p-type transistors used for CMOS design) will remain a cornerstone of electronic circuit design.

Many strategies exist to study and understand the behavior of microelectronic circuits and devices. Often the preferred methodology for beginning to understand a phenomenon is to measure its effects and to fit those result to a mathematical formula. Just as any periodic signal can be represented by a series of sinusoids, any functional phenomenon can be approximated by a sufficiently ordered polynomial. Describing the behavior of electronic devices with current and voltage equations uses the curve fitting approach; this method is fantastic for teaching electronic concepts and for practical design

of electronic circuits [2]. Compact modeling can even be extended as our understanding of electronic devices grows. In microelectronics, as device lengths shrink and more transistors fit on a single wafer, previously unobserved phenomena begin to affect the operation of these devices. Some examples are the effects of drain-induced barrier lowering (DIBL) and channel length modulation (CLM). The strategy taken in the compact modeling approach is to parameterize the functional models to include the contributions of these effects [3].

1.2 Computational Electronics

Clever parameterization schemes and modifications to the underlying equations allow compact modeling to predict the performance of electronic devices; however, these models tend not to describe the underlying physics of the devices. When there is a discrepancy between the predicted and actual behavior of a system, it can be important to understand the physics behind the relevant phenomena. While it is possible to understand the physics of a system purely through experimentation, analysis, and functional descriptions of observed behavior, it often helps to model the physics of a system directly. Computational electronics uses theoretical models that describe the physical behavior of electronic devices, experimental results that provide insight and key parameters for these models, and computational methods to predict the characteristics of these devices [4]. Figure 1 shows the synergy between experimental methods and various computational approaches used to study electronic devices and circuits.

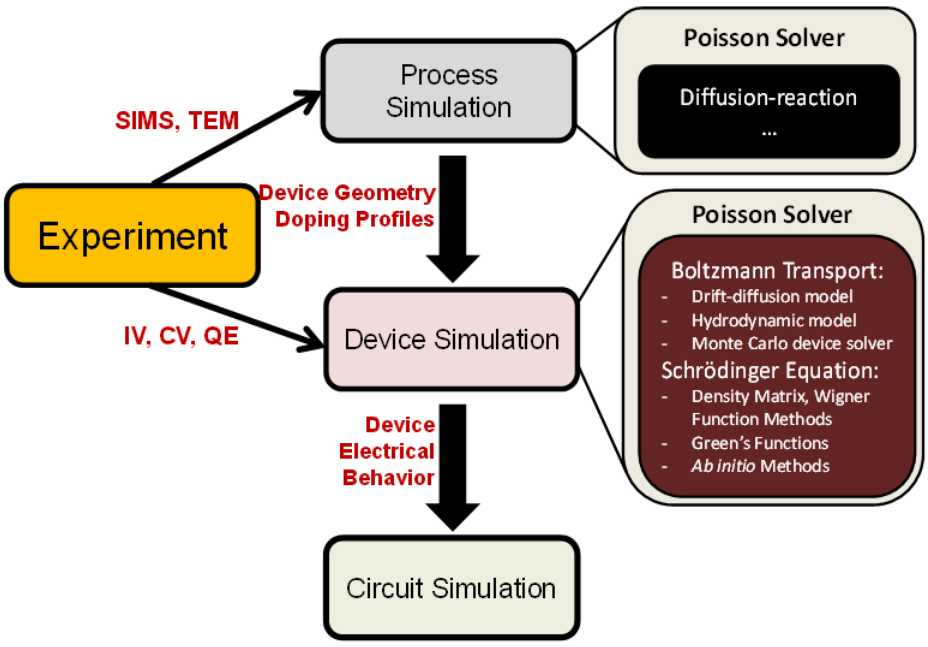

Figure 1 - Computational Electronics: Physical characterization such as secondary ion mass spectroscopy (SIMS) and transmission electron microscopy (TEM) inform semiconductor process simulation; electrical characterization such as current-voltage (IV) profiling, capacitance-voltage (CV) profiling, and quantum efficiency (QE) measurements inform semiconductor device simulation. The results of the process and device simulation improve simulation of circuit behavior.

When modeling the dynamics of a system, one must consider transport phenomena such as the exchange of mass, charge, energy or other physical quantities. Naturally, the study of electronic devices requires an understanding of charge transport. Device modeling methodologies make use of a variety of different transport models depending on the application; model selection is typically dictated by the scale of the device [5]. Figure 2 shows a hierarchy of charge transport models.

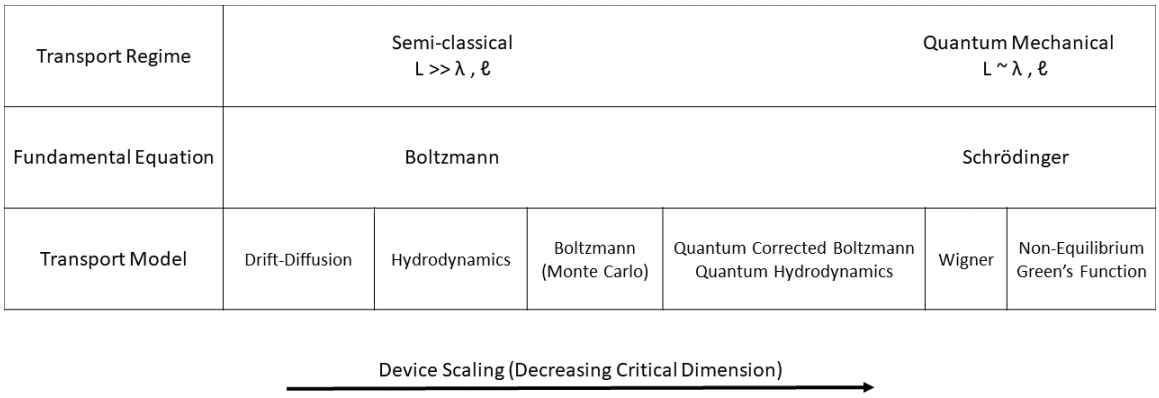

Figure 2 - Charge Transport Modeling Hierarchy: In the Semi-classical regime the characteristic length of the device (L) is much larger than the DeBroglie wavelength (λ) and the mean free path (ℓ). When the length scale is comparable with the DeBroglie wavelength and the mean free path, quantum mechanical models are appropriate.

Solving for device characteristics using these transport models typically follows the same basic protocol: computational techniques are used to solve the fundamental equations, which are supplemented by other equations that describe other important physical quantities. For example, it is common to solve the Boltzmann transport equation for charge transport while simultaneously solving Poisson's equation for the charge distribution and electric fields.

The use of modeling techniques to aid in the development of semiconductor device technology is known as Technology for Computer-Aided Design (TCAD). Many commercial TCAD tools are used in industry alongside compact modeling tools. Commercially available TCAD packages often rely heavily on one specific transport modeling methodology. To keep up with innovations in device topology, TCAD tools should use multi-scale strategies that incorporate the advantages and mitigate the disadvantages of each methodology [6]. This dissertation seeks to develop one such multi-

scale methodology to combine a particle-based solution to the semi-classical Boltzmann transport equation for charge transport with a fluid model for thermal transport.

Electrical characteristics are not the only factors in the behavior of microelectronic devices. Many other physical phenomena can be considered when studying these systems. Variations in the fabrication process can lead to non-uniformity in etched or deposited layers which can be modeled and predicted using process simulation. Defect chemistry determines how impurities and dopants behave within a crystal lattice and can be studied using molecular dynamics. Mechanical strain can affect the physical properties of the crystal lattice. Often individual phenomena are studied independently to better understand their effects, but sometimes they are studied alongside the charge transport models to determine electrical characteristics that account for the contributions of each phenomenon.

One such consideration of interest in microelectronics is the study of thermal transport. As transistor scaling drives devices further into the sub-micron lengths, not only are more precise charge transport models required, but so too are the effects of self-heating more pronounced. Microelectronic devices are typically operated by manipulating electric fields with applied voltage. Charge carriers gain energy as they accelerate in the presence of an electric field; this energy must go somewhere. Self-heating occurs when thermal energy is transferred from accelerated charge carriers to the crystal lattice. Charge transport modeling allows for the simulation of electrical characteristics and thermal transport modeling allows for the simulation of temperature effects [7]. Thermal modeling in electronic devices makes use of a variety of different techniques depending on the application. Figure 3 shows a hierarchy of thermal modeling; power density and electric field strength in critical device regions typically dictate model selection.

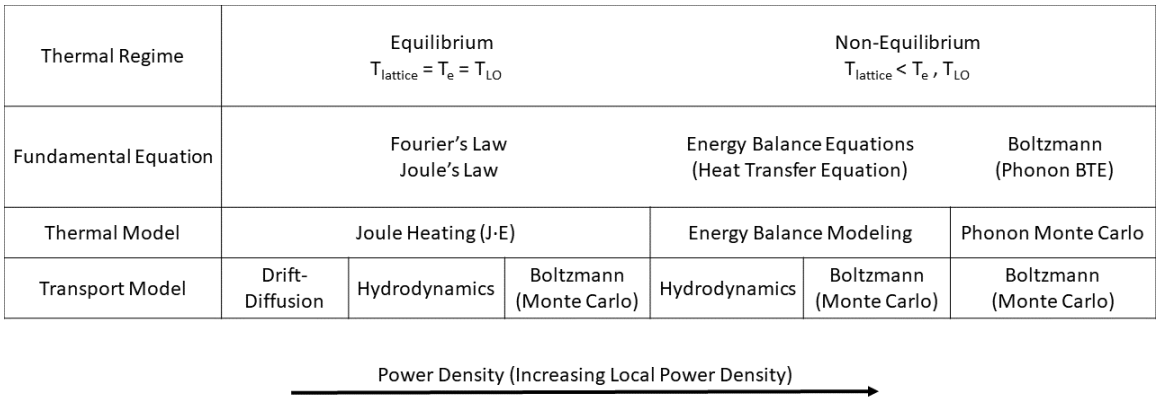

Figure 3 - Thermal Transport Modeling Hierarchy: In thermal equilibrium the temperature of the semiconductor ($T_{lattice}$), the charge carriers (T_e), and the phonons (T_{LO}) are equivalent. Hot-carrier effects drive the system into thermal non-equilibrium, where increased temperature of charge carriers and phonons must be considered.

The purpose of this dissertation is to establish a methodology for coupling thermal transport and charge transport modeling in MOSFET devices. A review of the literature on existing methods of electro-thermal simulation provides context for important considerations and explains the motivation for critical decisions made regarding this dissertation work.

1.3 Literature Survey

1.3.1 Drift-Diffusion Models Coupled to Appropriate Thermal Solvers

The first in the hierarchy of charge transport models is the drift-diffusion model, a semi-classical model derived by considering moments of the Boltzmann Transport Equation [4]. The drift-diffusion model is often favored for its relative simplicity because the current (density) at a given location is dependent only on the electric field and charge concentration gradient. Using the drift-diffusion model involves evaluating the current equations, continuity equations, and Poisson's equation. Many commercially available

TCAD tools use the drift-diffusion method to simulate device behavior. The drift-diffusion method can also be used for electro-thermal simulations; however, there is one critical limitation. Whereas particle-based models such the Monte Carlo method evaluate for individual carrier specific quantities for electrons and holes (i.e. carrier velocity, temperature, and location), the drift diffusion method only provides averages (e.g. drift velocity), densities (e.g. current density), and distributions (e.g. carrier distribution). Coupling the drift-diffusion method with thermal models is typically limited to the Joule heating (J·E) method. The current density is used to calculate the contribution of resistive heating, the effects of which appear as heat generation terms in the heat conduction equation.

Despite these limitations, the earliest attempts to couple charge transport and thermal transport models for semiconductor simulation use the drift diffusion and Fourier law method. One such paper discusses modeling thermal effects in BJTs in two dimensions. The flow of charge (current density) is determined using drift-diffusion equations, charge distribution is determined by solving the Poisson equation, and thermal effects are determined using the Joule heating (J·E) model [8]. The modeling techniques and methodologies have advanced significantly over the years, but the basic foundational methodology is still intact: solve for electrical characteristics and current flow, solve for thermal characteristics and heat flow, and couple the solvers in a meaningful and consistent way.

While electro-thermal coupling is restricted to the Joule heating method, there have been attempts at incorporating advanced thermal modeling alongside the relatively simple electrical characteristics of the drift-diffusion method. In one such paper electrical transport

is modeled using the drift-diffusion method and heat generation is derived as a function of the electrical quantities. Meanwhile, advanced thermodynamic models consider material thermal properties such as specific heat capacity and thermal conductivity alongside the heat generation terms derived from the electrical characteristics [9].

In addition to using the electrical characteristics to study the thermal effects in devices, there are also attempts to use the thermal results to improve the charge transport modeling. One such improvement is to incorporate temperature dependent mobility models which account for carrier self-heating. This technique has been applied to the study of self-heating effects in strained silicon semiconductor-on-insulator (SOI) devices [10]. The methodology includes a drift-diffusion simulation with temperature dependent mobility calculated using the relaxation time approximation (RTA). The self-heating included in these simulations is a modified resistive heating model that considers specific heat capacity, thermal conductivity, and thermal generation.

While most drift-diffusion based electro-thermal models use the Joule heating method, there have been attempts to modify the drift-diffusion equations to allow for other thermal transport models. One such paper studies electron transport and hot-electron interactions with optical and acoustic phonons in GaAs MESFETs [11]. The electron transport uses a modified drift-diffusion/Poisson solver; this couples with a thermal transport model that uses the energy balance equations for optical and acoustic phonons. This methodology considers the exchange of energy between electrons and phonons by substituting electrical properties from the drift-diffusion solution (e.g. concentration, drift energy, and drift velocity) into the energy balance equations for phonons. This scheme

accounts for the interaction of electrons with optical and acoustic phonons as well as phonon-phonon interactions between acoustic and optical phonons.

Many commercially available TCAD tools use the drift-diffusion method to simulate device behavior. One of the strategies commonly employed in electronics research is to use the available tools and incorporate custom solutions to mitigate the limitations of these tools. This approach is used to study thermal behavior in lateral double-diffused MOSFET transistors commonly used for high frequency and high-power applications [12]. The author makes a distinction between electrical non-equilibrium, where high electric fields cause a charge flux (current); and thermal non-equilibrium, where substantial temperature gradients and hotspots result from a difference in temperature between charge carriers and the crystal lattice. Predictably, electrical and thermal non-equilibrium are co-occurring in electrical devices, particularly in those with high electric fields and substantial power density. The study of these effects requires an electro-thermal model that allows for both electrical and thermal non-equilibrium. Using commercial TCAD tools (ATLAS) to gather electrical simulations results, importing quantities such as carrier concentration and carrier energy into a thermal solver, and evaluating thermal transport while considering these electrical characteristics provides such a framework. The thermal models used in this work are the energy balance equations for acoustic and optical phonons as well as the Joule heating model. In comparing the results of both heating models, the energy balance model predicts a more pronounced hotspot with larger temperature gradients than is predicted by the Joule heating model. This is a partially coupled solution; the results from the electrical characterization are input conditions for the thermal solver, but the thermal solution outputs do not couple back to the electrical solver.

Un-coupled or partially coupled methods of thermal simulation tend to underestimate the effects of self-heating [13]. Including the thermal effects as directly coupled to a particle-based device simulator, whether in the form of a coupled fluid model for phonon energy balance or a full phonon Monte Carlo, provides a much more accurate picture of the electro-thermal phenomena in micro- and nano- devices. The work of this dissertation improves significantly on this methodology by fully coupling the electrical and thermal solvers.

1.3.2 Hydrodynamic/Thermal Solver Coupling

One limitation of the drift-diffusion model is its inability to incorporate thermal effects beyond the Joule heating. The hydrodynamic model rectifies this assumption. Like the drift-diffusion model, the hydrodynamic model is derived from the Boltzmann Transport Equation.

Another problem that the hydrodynamic model addresses is the assumption that carriers travel at some saturation velocity within the drift-diffusion model under the force of an electric field. This assumption appears in compact models and drift-diffusion models in the form of carrier mobility terms. In compact model current equations, mobility is a constant, and the current is dependent on the applied voltage(s). In the drift diffusion model, the contribution from the drift term in the equation is dependent on mobility. Many drift-diffusion solvers use temperature dependent and field dependent mobility models to improve the results, but the underlying assumption remains. As charge carriers accelerate in the presence of an electric field, they often exceed the saturation velocity before settling. This is known as velocity overshoot. The effects of velocity overshoot cannot be considered when using a mobility-based model.

One strategy of implementing the hydrodynamic model is as an extension to the drift-diffusion equations as in the work of Majumdar et al. [11]. By deriving the equations of the hydrodynamic model, one arrives at a modified drift-diffusion equation which includes electron temperature. A similar strategy is used to modify the drift-diffusion equation by correcting the local drift velocity to account for velocity overshoot. Incorporating the results of increasingly complex models by modifying simpler models is a recurring theme in engineering.

Still it is possible to evaluate the equations of the hydrodynamic model without making such modifications or simplifications. This method is used to study self-heating effects in sub-micron silicon MOSFETs [14]. The methodology includes the hydrodynamic equation derived from the zeroth, first and second order moments of the Boltzmann transport equation (BTE), and a temperature dependent mobility model for electrons. Self-heating is included by solving for the interactions between high-energy electrons and the optical phonon modes; the thermal energy of the optical phonons is then assumed to decay into the acoustic modes. This offers a significant improvement over the resistive heating models and accounts for the separate interactions between hot carriers, acoustic phonon modes, and optical phonon modes.

1.3.3 Monte Carlo Device Simulations and Self-Heating

All the models discussed previously are continuum methods of describing the flow of charge in semiconductor devices. While current flow is often considered as a continuous phenomenon, it is made up of the contributions from individual charged particles. With small enough device dimensions, the continuous description of current becomes

inconsistent with reality, and a particle-based model becomes more desirable. In semiconductors the motion of charged particles (typically referred to as “charge carriers” or simply “carriers”) is determined by acceleration under the force of the electric field (drift), dispersion due to concentration gradients (diffusion) and random scattering events due to impurities, lattice vibrations, etc. In the drift-diffusion model, the effects of random scattering are incorporated in the mobility: carriers move at their saturated drift velocity as a function of the electric field, temperature, etc. In the hydrodynamic model, the effects of random scattering are incorporated through momentum and energy balance equations. The Monte Carlo method evaluates the effects of scattering directly by using stochastic techniques to select an appropriate mechanism and randomizing the momentum and energy of the scattered carrier accordingly.

Even so, the Monte Carlo method, like the drift-diffusion and hydrodynamic models, is based on the Boltzmann transport equation (BTE). Whereas the drift-diffusion and hydrodynamic models use moments of the BTE to derive a set of continuity equations, the Monte Carlo method satisfies the BTE by balancing the driving forces of drift and diffusion with the collision forces of random scattering. Deriving scattering rates according to Fermi’s golden rule and selecting random scattering processes according to these rates ensures that the Monte Carlo method satisfies the BTE in the long-time limit.

The Monte Carlo method is used for studying a variety of transport phenomena. It is commonly used to study charge transport, but it can be used for other particle-based studies as well. One such application is the study of electron transport in the context of surface spectroscopy [15]. To solve for electron transport in the context of semiconductor devices, the Monte Carlo solution to the BTE is coupled with Poisson’s equation or

Schrodinger's equation [16]. Tierney's dissertation work uses this methodology to study electron transport in HEMT and Spintronic devices. Device simulation using the Monte Carlo method is not limited to the study of electron transport. While electrons are the charge carriers most often associated with the flow of current, since they are responsible for current flow in conductors, other charged particles such as positively or negatively charged ions contribute to the flow of charge as well. In semiconductors, a valence state which is missing an electron is often considered a positively charged hole. Holes can move freely in the valence ban, much like electrons in the conduction band. The Monte Carlo method can thus be used to study hole transport in semiconductors.

The work of Dewey et al. gives an insight into the shortcomings of a parabolic band model – common in early Monte Carlo studies of electron transport – for studying hole transport [17]. To correct the errors, the parabolic band model is replaced with a piecewise continuous function for hole energy with respect to the wave vector; this technique is used for both the heavy hole and light hole bands. A parabolic spin-orbital band is included for simplicity. This dissertation uses a similar model for warping in the heavy hole and light hole bands, while using a parabolic band model for the split-off band.

While simplified band structure models (non-parabolic bands for electrons and warped bands for holes) are often sufficient, some methodologies instead use the full-band structure when simulating carrier transport. One such study uses the Monte Carlo method to solve for hole transport in silicon and germanium [18]. Instead of using a parabolic or warped band model for the valence band, this work uses the full-band structure to determine the distribution function and to calculate scattering rates in the valence band. The pseudopotential method along with Cohen and Bergstresser's atomic pseudopotentials

is used to determine the band structure [19]. Scattering rates are derived using Fermi's golden rule. While this provides a great basis for studying hole transport in the valence band of silicon and germanium, it does not appear to provide a significant advantage over the warped band model used in other works.

The insights from Monte Carlo studies can also be used to improve our understanding of the underlying behaviors governing device performance. One such effort uses a full-band Monte Carlo simulation to study bulk valence-band transport properties in silicon and germanium [20]. The band structure is calculated using the k·p method and the scattering is calculated using Fermi's golden rule. The focus of this paper is to understand the dependence of the ohmic mobility on the optical deformation potential, and to use this understanding to predict the temperature dependence of the ohmic mobility. This work seems critical for developing temperature dependent mobility models to use in conjunction with drift-diffusion based devices simulators. The device simulator presented in this dissertation work uses the particle-based Monte Carlo directly to study transport in the device so there is no need to extract bulk parameters such as mobility.

While the Monte Carlo method has the inherent advantage of directly modeling the behavior of carriers under the influence of random scattering, it has advantages in electro-thermal modeling as well. While the drift-diffusion model is limited to studying thermal transport using the Joule heating method and the Fourier law, the Monte Carlo method does not have this limitation. Still, the Fourier law can be used alongside the Monte Carlo method to study thermal effects. One such effort studies an interesting device structure of strained silicon MODFETS [21]. The simulation methodology is to couple a Monte Carlo solver for electrical transport with a heat diffusion equation solver for thermal transport.

This is a reasonable methodology since it allows the coupling of the Monte Carlo solver to the thermal solver in the form of heat generation sources based on the electrical analysis from the Monte Carlo. The Monte Carlo – if it allows for temperature dependent scattering – can be coupled with temperature profile from the thermal result. The only phenomena this methodology cannot account for are local thermal non-equilibrium effects: the effects of the electron-phonon and phonon-phonon interactions that occur when there is a discrepancy in local temperature between electrons, acoustic phonons, and optical phonons. With the significant difference in lifetime and mean free path of optical and acoustic phonons, this can play a significant role in thermal transport. The work of this dissertation addresses these effects by solving for the energy balance equations for phonons rather than the Fourier law for heat flux.

The Monte Carlo method can comfortably address the contributions from local thermal non-equilibrium effects. Since it is a particle-based methodology, the Monte Carlo method is ideal for studying phenomena that exhibit localized effects. Individual particle parameters and locations within the device are already tracked when solving using the Monte Carlo method; the inclusion of carrier temperature as one of these parameters allows for a difference in local temperature between electrons, acoustic phonons, and optical phonons. This fact provides the basis for a methodology of simulating thermal effects in nanodevices by coupling the particle-based Ensemble Monte Carlo (EMC) solution to the Boltzmann Transport Equation (BTE) for electrons with a fluid model for optical and acoustic energy transfer derived from the BTE for phonons [13]. Similar techniques have been used to study electron transport in silicon semiconductor-on-insulator (SOI) devices [22], [23] and nanowire devices [24]. The same methodology can be adapted for particle-

based simulation of both electron and hole transport coupled with the fluid model for thermal energy transfer.

1.3.4 Phonon Monte Carlo and Miscellaneous Electro-Thermal Effects

Several studies approach electro-thermal modeling using methodologies that differ from those described above. Artaki's study of hot phonon effects in silicon field effect transistors (FETs) is one such example, which considers the effects of non-equilibrium electron temperature on bulk phonons in silicon [25]. The formulation assumes a quasi-classical and locally Maxwellian distribution of electrons with a temperature significantly greater than that of the lattice temperature. Bulk phonons are assumed to equilibrate with the hot electrons locally; this equilibration is treated by solving Planck's formula for electrons and phonons. The electron temperature is calculated as a function of the electric field using a field dependent mobility model. Finally, the energy loss of hot electrons though phonon assisted thermalization is calculated as a function of the electric field. This establishes a theoretical framework for determining the contribution of phonon scattering effects on energy loss in charge carriers in bulk silicon.

Thermal modeling is not limited to Fourier's law or the energy balance method. Rather than treating thermal transport as a continuum phenomenon, it is possible to treat individual lattice vibrations (phonons) as particles and calculate their transport characteristics accordingly. Optical and acoustic phonons follow the Boltzmann transport equation for phonons. There are many ways to evaluate the phonon BTE; lower order moments of the phonon BTE simplify to Fourier's law and the energy balance equations. These methods of evaluation were discussed in the previous sections.

The phonon BTE can also be evaluated stochastically using the Monte Carlo method; Ramayya used this method to study thermoelectric properties of silicon nanowires [26]. A 1-D phonon Monte Carlo solves for thermal transport while a coupled 1-D Poisson-Schrödinger solver evaluates charge transport. Further studies of phonon Monte Carlo are included in the thesis work of Abdul Shaik, where the results of the phonon Monte Carlo show that bulk conductivity models are insufficient in describing thermal behavior in nanoscale devices [27].

These studies on phonon Monte Carlo techniques provide a pathway for advanced progression of electro-thermal modeling in nanoscale devices. Expanding the capabilities of such solvers to allow for 2- and 3-dimensional solutions and coupling with compatible Poisson-Boltzmann or Poisson-Schrödinger solvers will allow for simulation of advanced device structures.

1.4 Purpose and Project Scope

The purpose of this dissertation is to present the cumulative results of a research study in the topic of electro-thermal simulation of CMOS devices and circuits. This study uses the ensemble Monte Carlo technique of solving the Boltzmann transport equation (BTE) for charge transport alongside the energy balance method for evaluating thermal transport. Prior results demonstrate the feasibility of this method for modeling CMOS circuits in two parts: electro-thermal simulation of NMOS devices and electrical simulation of a CMOS inverter. This dissertation prioritizes coupling of the electro-thermal solver with the CMOS solver.

The thermal solver, which uses the energy balance equations to determine optical and acoustic phonon temperatures, shows reliable results while coupled to the electron

Monte Carlo device simulator and used to solve for NMOS device performance. The goal of this dissertation is to couple the thermal solver with the electron-hole Monte Carlo device simulator to solve for CMOS device behavior and circuit performance. Implementing the coupled solver requires introducing temperature dependent scattering tables for both electrons and holes. In addition to calculating the temperature dependent scattering tables, each simulation subroutine that handles ensemble particles or particle attributes must be compatible with the additional temperature parameters. Finally, the energy balance solver evaluates the thermal transport using the temperature parameters from the electron-hole Monte Carlo.

Coupling the energy balance solver with the electron-hole Monte Carlo device simulator follows the same procedure as coupling with the electron Monte Carlo device simulator. Electrical parameters - carrier temperature, carrier concentration, and average velocity - from the device solver couple with the thermal solver to evaluate the energy balance equations. Finally, the entire coupled electro-thermal code is verified while using both the temperature dependent scattering mechanisms for the Monte Carlo and the optical and acoustic phonon temperatures from the energy balance solver. Results are consistent with those previously shown in the literature, but with some degradation in device performance due to carrier self-heating. Results also provide insight into the difference in thermal behavior of NMOS and PMOS devices.

After implementing the coupled electro-thermal solver for CMOS devices, the next step is to generalize the simulator for CMOS circuit applications. Simulating CMOS circuits using a single generalized solver requires that the Monte Carlo solution to the Boltzmann transport equation (BTE) include both electrons and holes in the particle

ensemble. The electrical device solver for CMOS can simulate the behavior of a CMOS inverter. The electro-thermal device solver provides insight into how the effects of carrier self-heating affect circuit performance.

In the future it will be beneficial to address the issue of continuity methods. The results shown in this dissertation use a brute force method of maintaining current continuity in CMOS circuits connected in series. Revisiting injection and extraction methods of continuity modeling could provide a more robust means of studying CMOS systems.

The motivation for this dissertation is to study practical applications of multi-scale modeling approaches. The generalized CMOS electro-thermal simulator described in this dissertation could eventually be coupled with a global multi-scale solver for the heat flow in the surrounding material and interconnects. This would provide a robust and versatile platform on which to study carrier self-heating, the effects of closely spaced adjacent devices, and heat flow in the surrounding circuitry. The simulations shown in this dissertation provide some insight as to how self-heating affects device performance. A full multi-scale solver which incorporates the dual carrier electro-thermal solver might provide even more. The NMOS global multi-scale device-and-interconnect solver shown in this dissertation demonstrates the feasibility of such a tool.

This dissertation prioritizes the development and testing of a CMOS device solver compatible with this global multi-scale methodology; coupling with the global solver is outside the scope of this dissertation project.

CHAPTER 2

THE MONTE CARLO METHOD

2.1 Charge Transport

Effective modelling of the behavior of electronic devices requires accurately describing carrier transport. In the case of Silicon MOSFETs, electron and hole transport in the channel determines the flow of current in the device. There are several options, shown in Fig. 4, for calculating carrier transport in semiconductors: drift-diffusion, hydrodynamics, Boltzmann, Wigner, and Green's functions. Both hydrodynamics and Boltzmann methods also come in quantum corrected varieties while Green's functions can be solved in equilibrium, near-equilibrium and non-equilibrium cases. This dissertation uses the Monte Carlo method of solving the Boltzmann transport equation (BTE).

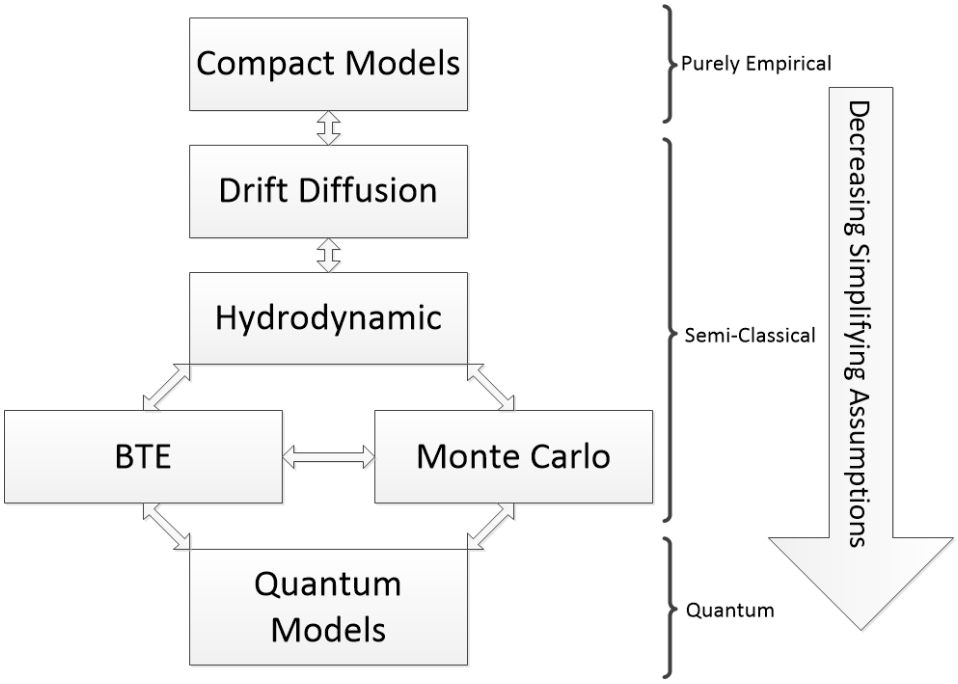

Figure 4 - Semiconductor Modeling Techniques: This hierarchy of modeling techniques is arranged according to the number of simplifying assumptions needed. This dissertation focuses on the Monte-Carlo/Boltzmann Transport methodology.

2.2 The Boltzmann Transport Equation

To solve the BTE using the Monte Carlo method, the BTE is arranged such that drift and diffusion processes or driving forces are balanced by the scattering processes or diffusive forces. Particle motion due to the electric field and concentration gradient is described by differential terms. Particle motion due to interactions with other particles, impurities in the semiconductor, and the crystal lattice is described by the collision integral. The BTE in this form allows for the stochastic evaluation of charge carrier transport.

$$\frac{\partial f(\mathbf{r},\mathbf{v},t)}{\partial t} = -\mathbf{v}\cdot\nabla_r f - \frac{\mathbf{F}}{m}\cdot\nabla_v f + \left.\frac{\partial f}{\partial t}\right|_{Coll} + \left.\frac{\partial f}{\partial t}\right|_{G-R} \tag{1}$$

Equation (1) is a generalized form of the BTE. The generation and recombination (G-R) terms cannot be treated using the Monte Carlo method because the time scale for these processes differs sufficiently from that of the collision processes. The Monte Carlo method for solving the BTE becomes insufficient in devices such as bipolar junction transistors (BJTs) where generation and recombination contribute significantly to carrier transport dynamics. In devices such as field effect transistors (FETs) the G-R terms are negligible in the transport dynamics. Several classical quantities must be replaced with the appropriate quantum terms to describe the effect the semiconductor band structure has on carrier transport.

$$\frac{\partial f(\mathbf{r},\mathbf{k},t)}{\partial t} = -\frac{1}{\hbar}\nabla_k E(k)\cdot\nabla_r f - \frac{\mathbf{F}}{\hbar}\cdot\nabla_k f + \left.\frac{\partial f}{\partial t}\right|_{Coll} \tag{2}$$

Equation (2) shows the form of the BTE derived when omitting the G-R terms and substituting the appropriate quantum quantities. Evaluating this form of the BTE using the

Monte Carlo method gives a reliable semi-classical model for transport of electrons and holes in semiconductor materials.

2.3 The Monte Carlo Method for Solving the BTE

2.3.1 Methodology

Solving the differential terms of the BTE can be simplified by solving in the quasi-static regime. In digital logic circuits, this approximation can be justified since the rate of change in the electric field and concentration gradients are relatively low in comparison with the same parameters in high speed devices, such as high frequency amplifiers or radio frequency devices. When solving in the quasi-static regime, the effect of the electric field on a charge carrier is simplified as a constant force applied over a small enough time step. Newton's second law determines the acceleration of the charge carrier based on the effective mass in the conduction band, the amount of charge (±q), and the magnitude of the electric field. If the time-step is selected appropriately such that the electric field seen by the charge carrier is approximately constant, this quasi-static simplification can be applied to dynamic systems.

The collision integral is solved by calculating scattering rates and using the Monte Carlo method to select an appropriate scattering mechanism stochastically. By allowing each charge carrier to accelerate under the force of the electric field, and then to scatter according to the appropriate statistical model, this methodology assures that both sides of the BTE are balanced and the transport is described accurately.

2.3.2 Carrier Free-Flight

The Monte Carlo method assumes the motion of each particle consists of finite free-flight terminated by a scattering event which changes momentum and energy of the particle. Free-flight times for each particle are generated randomly according to probability functions related to the scattering rates. Simulating an ensemble of particles requires synchronizing the free-flight potion of the Monte Carlo method without sacrificing the probabilistic nature of the random flight times. Introduction of a simulation time step allows for this synchronization. If an ensemble particle has a cumulative free-flight time that exceeds the prescribed time step, the particle accelerates under the force of the electric field for the duration then awaits the start of the next time step. If an ensemble particle scatters before the end of the prescribed time step, the outcome of the scattering event is resolved, and a new free-flight time is calculated; this repeats until each particle in the ensemble has enough cumulative free-flight time to reach the end of the time step.

In a bulk Monte Carlo simulation, the force acting on each particle during free-flight is from an external electric field, defined in the simulation parameters. Adjusting the external electric field and monitoring the response of the ensemble particles allows for the evaluation of bulk charge transport properties. The Monte Carlo simulation computes the energy, momentum, and velocity of each particle in the ensemble. Comparing the saturation velocity against a range of external field values allows for the calculation of field dependent bulk mobility. Observing the transient behavior as carriers approach their saturation velocity provides insight regarding velocity overshoot. In a Monte Carlo based device simulator, there are internal electric fields acting on the particles during free-flight that are calculated separately.

2.3.3 Scattering Rates

Appropriate treatment of scattering phenomena in the Monte Carlo simulation ensures that the interactions described by the collision term in the BTE balances with the driving forces described by the differential terms. Scattering rates are necessary to construct the probability density functions used to randomly select the free-flight time. Scattering rates are also necessary to determine the final state of each particle after scattering occurs. The scattering rates used in Monte Carlo simulations depend on the band structure of the semiconductor. Figure 5 shows an illustration of the silicon band structure.

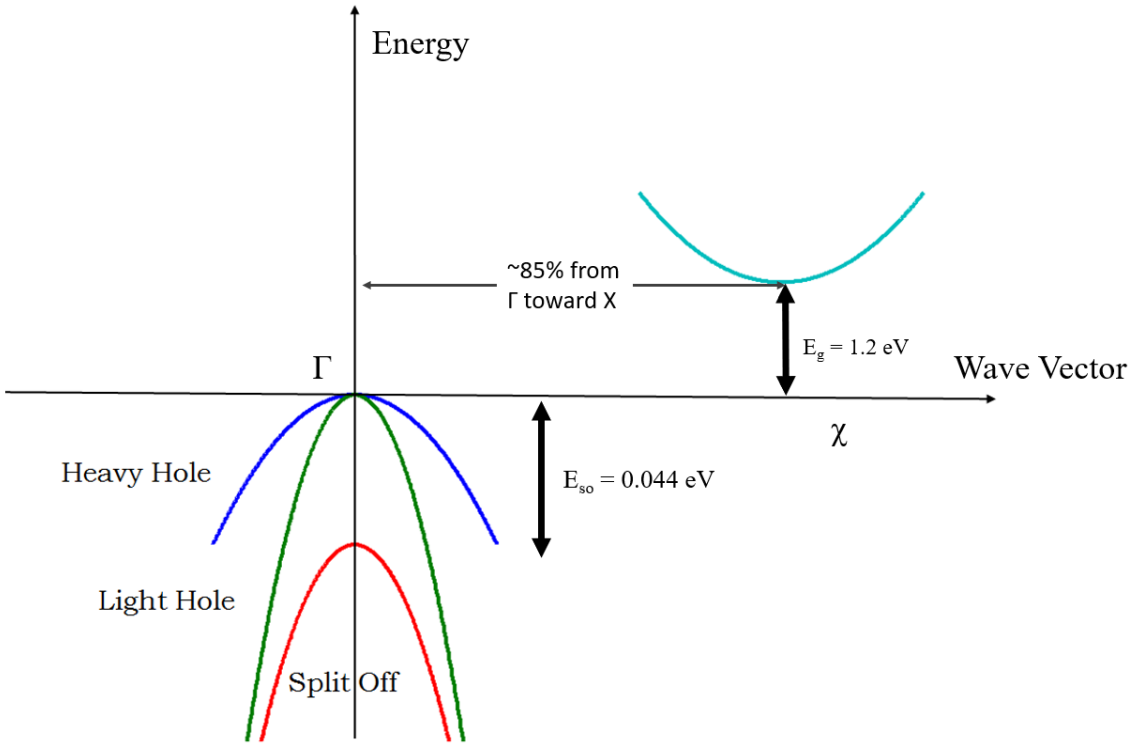

Figure 5 - Silicon Band Structure: The illustrated band structure of silicon shows the lowest energy conduction band valley and three valence bands. This dissertation considers electron transport in this conduction valley and hole transport in these three valence bands.

Conduction band scattering calculations use a non-parabolic band approximation to provide a more accurate dispersion relation. Valence band scattering calculations use a warped band approximation because the parabolic approximation fails to accurately describe the dispersion relation for holes. Several scattering phenomena are included in the calculation of the scattering tables. Acoustic phonon intra-band scattering is included for both electrons and holes. Acoustic and optical phonon inter-band scattering is also included for both electrons and holes, but the difference in dispersion relations between the conduction and valence bands necessitates unique considerations of electrons and holes.

Electrons in the conduction band occupy the valley located near the X-point in the first Brillouin zone, meaning there are six equivalent valleys; this is illustrated in Fig. 6a. Because of the k-space orientation of these equivalent valleys, inter-band scattering can occur in one of two processes: an f-process occurs when an electron scatters into a valley along an orthogonal axis relative to the starting valley, a g-process occurs when an electron scatters into the opposite valley along the same axis relative to the starting valley.

Holes in the valence band are assumed to occupy one of three energy bands: heavy hole, light hole, and split-off. All three are centered around the gamma-point in the Brillouin zone. The heavy hole and light hole band occur at the gamma-point and their dispersion relations are described using the warped band approximation; warping in the valence band is illustrated in Fig. 6b. The split-off band is also centered at the gamma-point, but with greater energy separation.

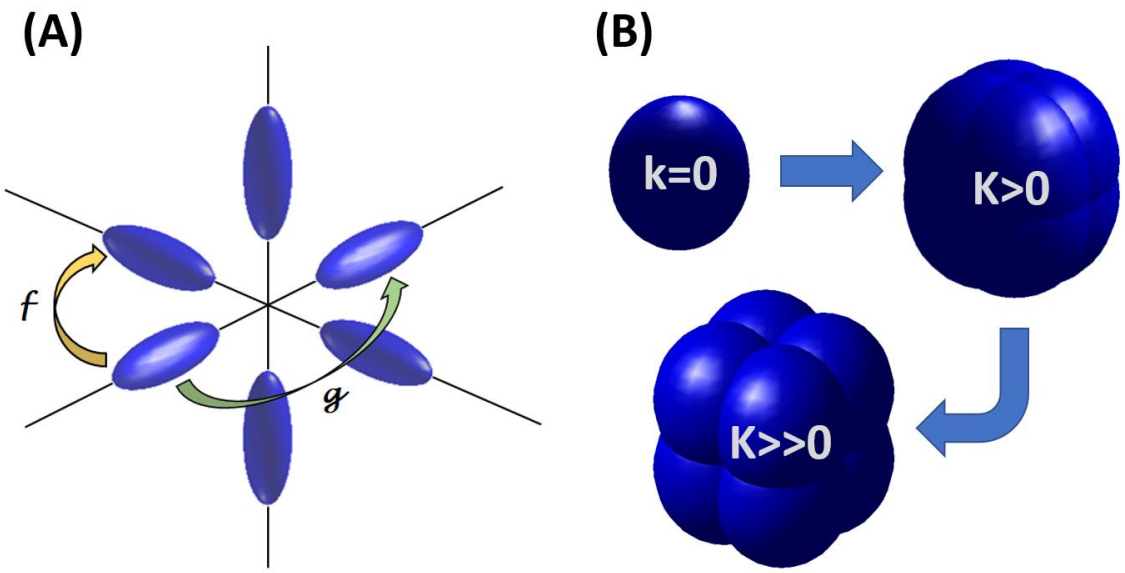

Figure 6 - Conduction and Valence Constant Energy Surfaces: (A) The silicon conduction band has six equivalent valleys about the X-point. Inter-valley scattering rates must account for two types of scattering processes in these valleys. (B) Heavy hole and light hole valence bands in silicon exhibit warping. Constant energy surfaces are approximately spherical near to the gamma point but become increasingly warped as energy increases. The

Coulomb scattering occurs due to attractive or repulsive forces between mobile charge carriers and immobile charge ions in the crystal lattice. Ionized donor or acceptor dopant atoms, charged defects in the crystal, dangling bonds at material interfaces, and other forms of impurities can cause Coulomb scattering. Without simulating the molecular dynamics of the system or introducing an interface charge profile, it is still possible to account for ionized impurity scattering due to donor and acceptor doping. Coulomb scattering is included for electrons, but not for holes. The scattering tables for electrons and holes in silicon are shown below in Fig. 7-10.

Table 1: Phonon Deformation Potentials in Silicon Conduction Band

Scattering Process	Type of Phonon	Temperature (K)	Energy (meV)	Deformation Potential (10^8 eV/cm)
f1	TA	220	19	0.5
f2	LA/LO	550	51	3.5
f3	TO	685	57	1.5
g1	TA	140	10	0.3
g2	LA	215	19	1.5
g3	LO	720	62	6

The deformation potentials in Table 1 are used to calculate the intervalley phonon scattering rates for electrons in the conduction band [28].

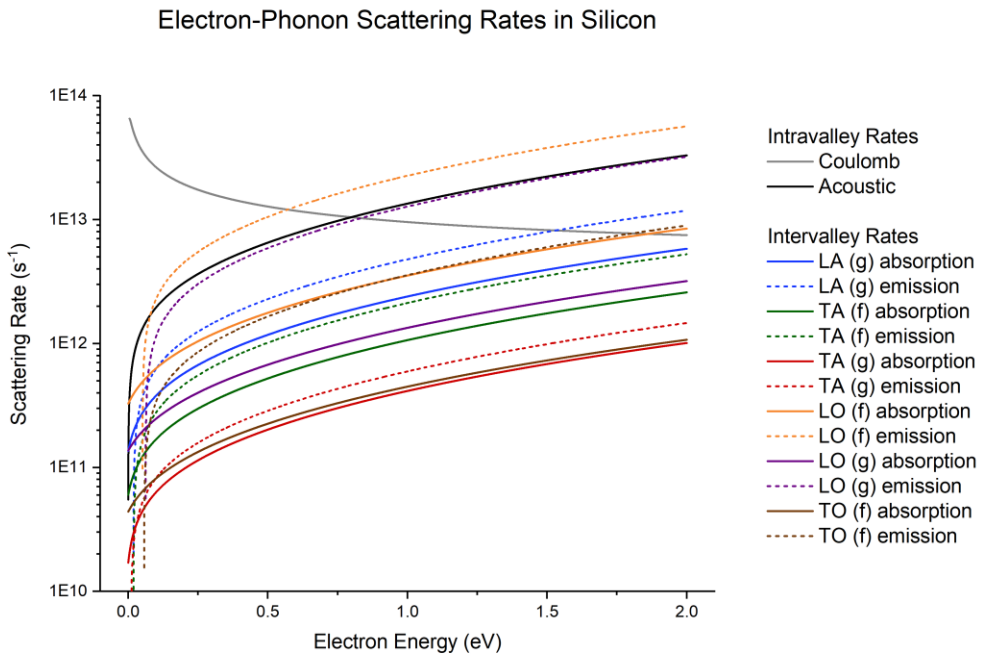

Figure 7: Electron-phonon scattering rates in in silicon.

Table 2: Piecewise Non-Parabolic Description of Warped Valence Bands

Band	Energy Range (eV)	Wavevector Range (10^8 cm^{-1})	Non-Parabolicity (eV^{-1})	Effective Mass	Energy Offset (eV)	Wavevector Offset (10^8 cm^{-1})
Heavy Hole	0 - 0.5155	0 - 0.404	0.4	1	0	0
	0.5155 - 2	> 0.404	0	-1.4124	0.9558	0
Light Hole	0 - 0.2	0 - 0.1259	0.1	0.2	0	0
	0.2 - 1.1	0.1259 - 0.3398	0	-1.0736	1.7392	0.7642
	1.1 - 2	> 0.3398	-0.045	0.9	0.6	0
Split-Off	0.044 - 2	≥ 0	0	1	0	0

The piecewise non-parabolic description described in Table 2 is used to calculate the intervalley phonon scattering rates for holes in the valence band [29].

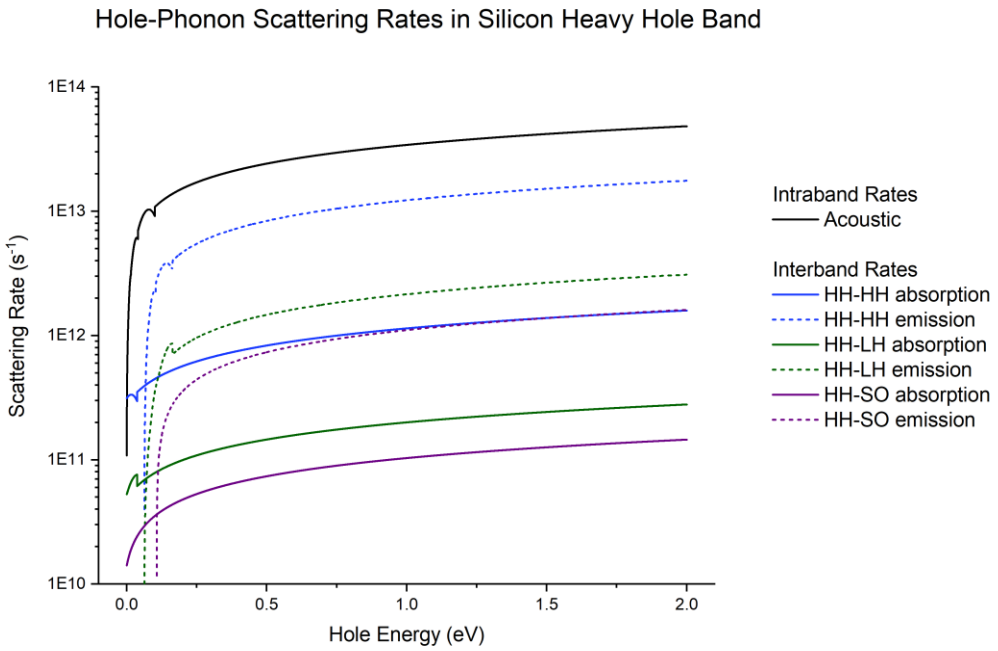

Figure 8: Hole-phonon scattering rates in the heavy hole band in silicon.

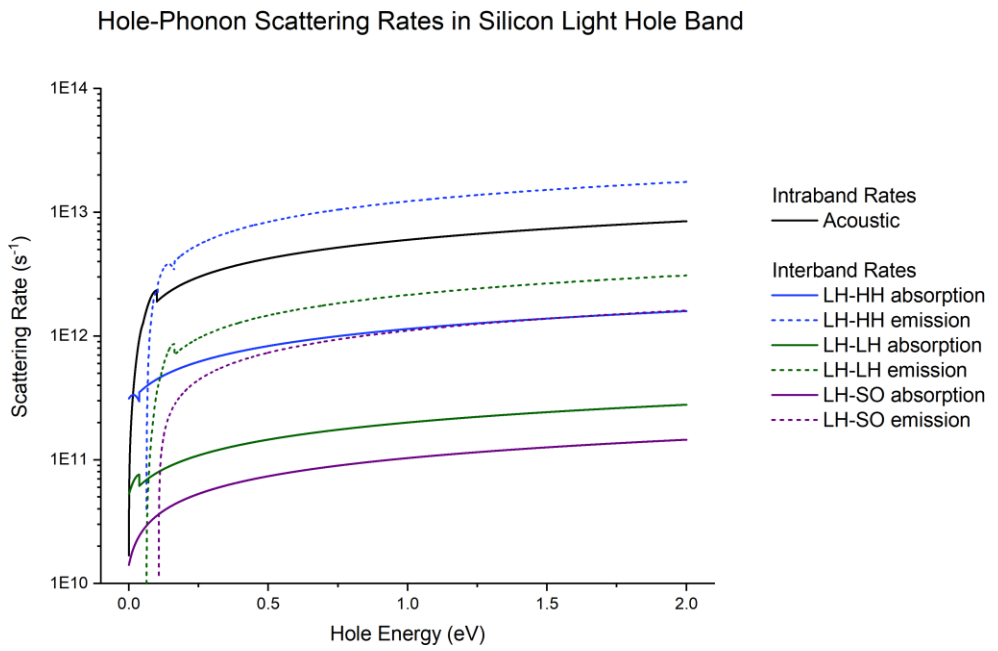

Figure 9: Hole-phonon scattering rates in the light hole band in silicon.

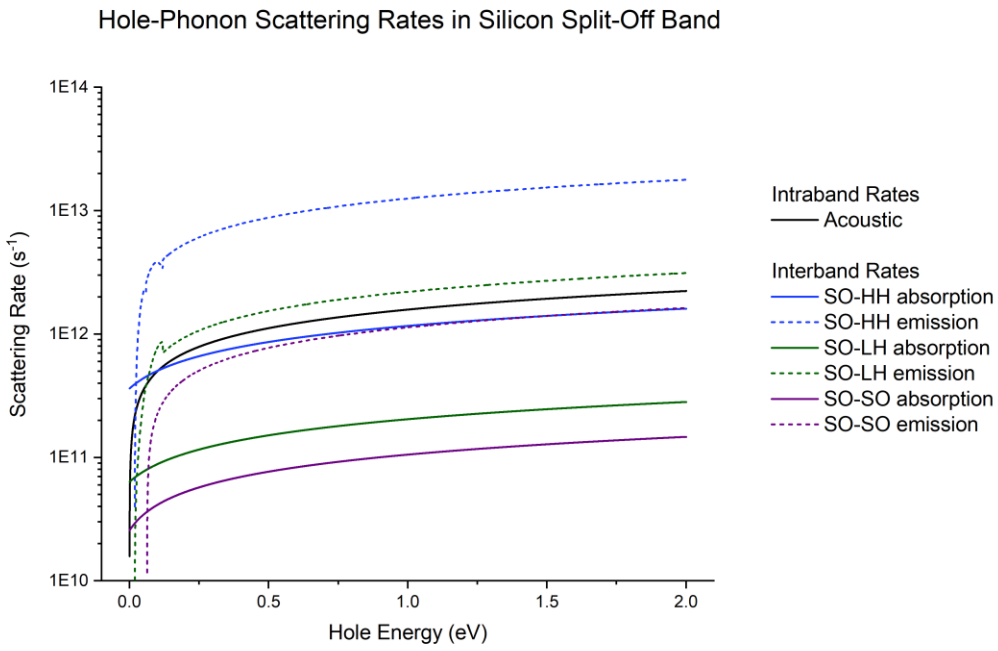

Figure 10: Hole-phonon scattering rates in the split-off band in silicon.

2.4 Bulk Mote Carlo Results

Bulk Monte Carlo simulations are used to evaluate bulk properties in semiconductors by solving the BTE for charge transport. These bulk properties provide valuable insight about the material systems present in semiconductor electronics. Figure 11 shows bulk results for holes in silicon.

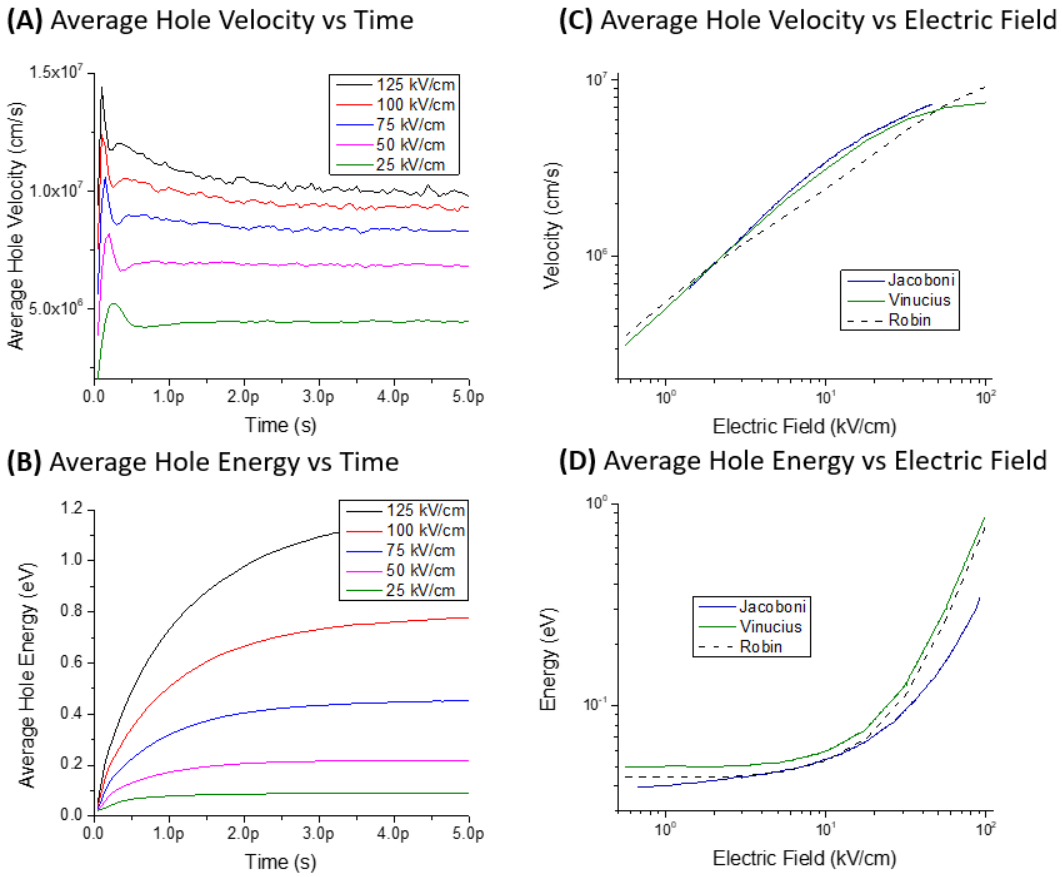

Figure 11 - Bulk Hole Monte Carlo Simulation Results: Velocity versus time (A) and energy versus time (B) show the transient behavior of holes in the bulk simulation. Velocity versus electric field (C) and energy versus electric field (D) characteristics are compared against existing results in the literature (Jacoboni) and collaborators (Vinucius) to verify the performance of the Monte Carlo simulator.

These bulk Monte Carlo Results are useful in studying behavior of materials used in semiconductor device manufacturing. Often Monte Carlo results can be used to extract key parameters for use with other types of models. For example, it is common to use bulk

Monte Carlo results to generate field dependent mobility models for use with a drift-diffusion solver. This method is vital to extending the useful lifetime of existing reliable modeling techniques while novel – but often less reliable – techniques are developed.

The focus of this work; however, is to develop a device solver based on the Monte Carlo method of solving the BTE for charge transport. The Monte Carlo evaluates for the particle motion and scattering (known as the carrier free-flight/scatter loop) in the presence of an electric field. In the bulk solver, the electric field is a constant applied field, irrespective of position. In a semiconductor device the electric field arises as a result of an applied voltage bias and the field varies with position; additional techniques are required in order to calculate the electric field for the device solver.

CHAPTER 3

PARTICLE BASED DEVICE SIMULATOR

3.1 Spatial Quantities in the Device Structure

The Monte Carlo method for solving the Boltzmann Transport Equation (BTE) provides a solution for charge carrier transport in a semiconductor bulk crystal with a constant electric field. To simulate carrier transport in a micro-electronic device, one must describe the structure of the device and calculate the magnitude of the electric field throughout. Under appropriate conditions, a quasi-static description of the electric field accurately models the drift forces contributing to carrier transport. For each time step in the simulation, an electro-static "snap-shot" of the device provides the necessary parameters. This "snap-shot", acquired by solving Poisson's equation for electrostatics, gives the electric potential. Solving for the gradient of the potential gives the electric field as a function of position [4].

Many parameters evaluated as scalars in the bulk Monte Carlo solver become time and position dependent variables in the device simulator. Quantities such as doping density, carrier concentration, and electric field, treated as constants in the bulk simulator, vary with position, and/or time in the device simulator. This difference necessitates the careful construction of a spatial mesh, illustrated in Fig. 12, for mapping quantities to real-space coordinates. Defining the characteristics of this mesh is critical in describing the device structure.

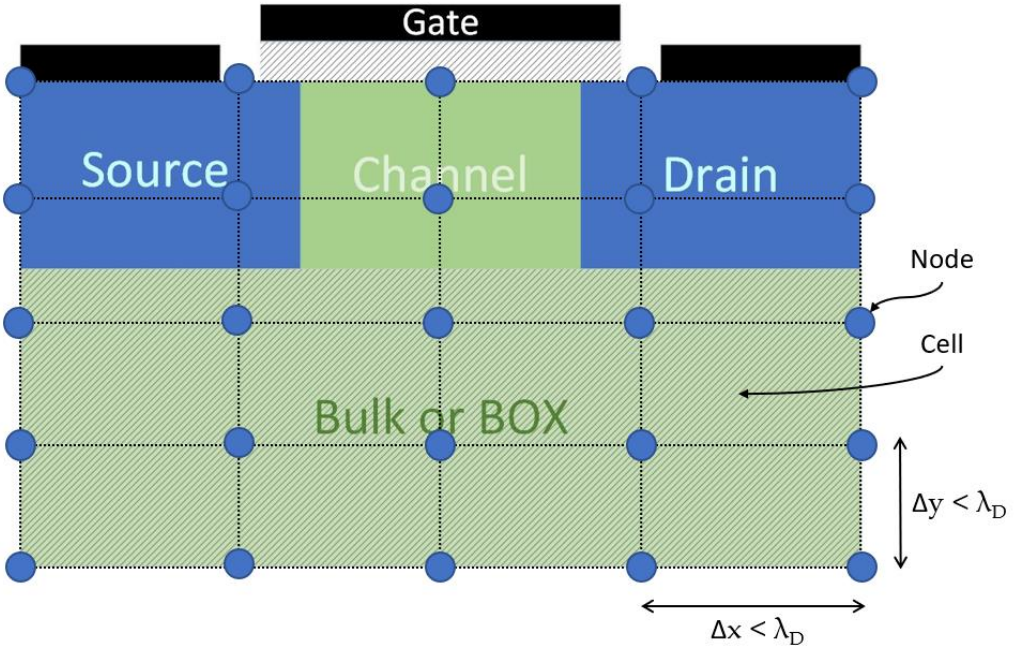

Figure 12 - Device Structure and Mesh Illustration: This is a qualitative depiction of the rectangular mesh used to define a device structure. Material parameters and several evaluated quantities, such as electric potential, are mapped to the nodes. Spatial quantities not mapped to nodes, such as electric field and particle position, occupy cells between nodes. The node spacing (Δx and Δy) must be smaller than the smallest wavelength of the charge variation, approximated by the Debye length (λ_D). This mesh facilitates the numerical methods used in simulation and adheres to the physical structure of the device.

A rectangular mesh facilitates a straightforward numerical solution to Poisson's equation. Uniform node spacing makes locating ensemble particles within the mesh trivial. Node spacing less than the Debye length ensures that the quasi-static approach gives a reasonable approximation of the transport dynamics. Device parameters such as doping concentration are defined at the nodes. Material parameters such as electric permittivity are

defined within each cell. The Poisson equation is evaluated for the electric potential along the nodes while the electric field is calculated within each cell [30].

3.2 Solving the Poisson Equation

Poisson's equation emerges from evaluating Gauss's Law in the electrostatic approximation. Gauss's law states that the divergence of the displacement vector (**D**) is equal to the free charge density (ρ).

$$\nabla \bullet \mathbf{D} = \rho \tag{3.1}$$

In a linear, isotropic, and homogeneous material, the displacement vector is the product of the permittivity (ε) and the electric field.

$$\mathbf{D} = \varepsilon \mathbf{E} \rightarrow \nabla \bullet \mathbf{E} = \frac{\rho}{\varepsilon} \tag{3.2}$$

Faraday's law states that the curl of the electric field is equal to the negative time rate of change of the magnetic field ($\partial\mathbf{B}/\partial$t). In the absence of a magnetic field, the curl of the electric field is zero, and the electric field can be described as the negative gradient of a scalar potential function (φ).

$$\nabla \times \mathbf{E} = -\frac{\partial \mathbf{B}}{\partial t} = 0 \rightarrow \mathbf{E} = -\nabla \varphi \tag{3.3}$$

Substituting the result of Equation 5 into Equation 4 gives Poisson's equation.

$$\nabla \bullet \mathbf{E} = \nabla \bullet (-\nabla \varphi) = \frac{\rho}{\varepsilon} \rightarrow \nabla^2 \varphi = -\frac{\rho}{\varepsilon} \tag{3.4}$$

Evaluating for the electrostatic potential in regions of spatially varying permittivity requires the generalized form of Poisson's equation.

$$\nabla \bullet (\varepsilon \nabla \varphi) = -\rho \tag{3.5}$$

The equation is linearized and discretized so that the potential at each node can be evaluated iteratively using a five-point stencil, shown in Fig. 13. The resulting system of linear equations are solved using the successive over-relaxation (SOR) method.

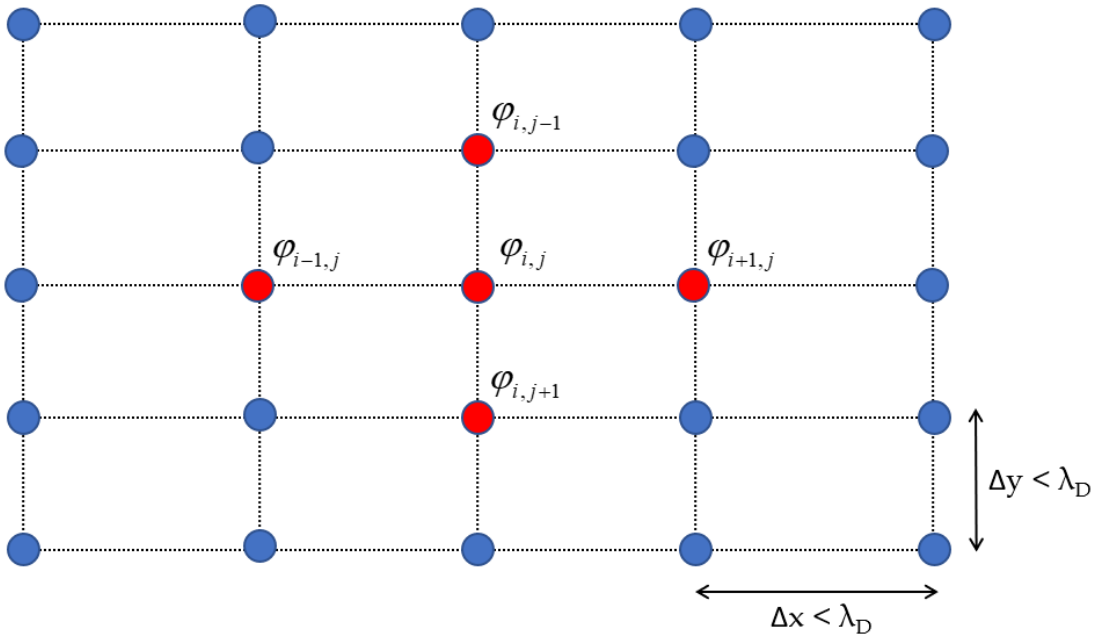

Figure 13 - Five-Point Stencil for Solving Poisson's Equation: Indices i and j allow for the identification of each node within the mesh. Solving for the potential, $\varphi_{i,j}$, at the central node relies on values of the potential in the adjacent nodes.

The potential is calculated using the finite difference discretization.

$$\nabla^2\varphi(i,j) = \frac{\partial^2\varphi(i,j)}{\partial x^2} + \frac{\partial^2\varphi(i,j)}{\partial y^2} = -\frac{\rho(i,j)}{\varepsilon} \tag{3.6}$$

$$\frac{\partial^2\varphi(i,j)}{\partial x^2} \approx \frac{\varphi(i-1,j) - 2\varphi(i,j) + \varphi(i+1,j)}{(\Delta x)^2} \tag{3.7}$$

$$\frac{\partial^2 \varphi(i,\, j)}{\partial y^2} \approx \frac{\varphi(i,\, j-1) - 2\varphi(i,\, j) + \varphi(i,\, j+1)}{(\Delta y)^2} \tag{3.8}$$

$$\frac{\varphi(i-1,\, j) - 2\varphi(i,\, j) + \varphi(i+1,\, j)}{(\Delta x)^2} + \frac{\varphi(i,\, j-1) - 2\varphi(i,\, j) + \varphi(i,\, j+1)}{(\Delta y)^2} = -\frac{\rho(i,\, j)}{\varepsilon} \tag{3.9}$$

$$(\Delta y)^2 \varphi(i-1,\, j) - 2(\Delta y)^2 \varphi(i,\, j) + (\Delta y)^2 \varphi(i+1,\, j) +$$

$$(\Delta x)^2 \varphi(i,\, j-1) - 2(\Delta x)^2 \varphi(i,\, j) + (\Delta x)^2 \varphi(i,\, j+1) = -\frac{(\Delta x)^2 (\Delta y)^2 \rho(i,\, j)}{\varepsilon} \tag{3.10}$$

$$\varphi(i,\, j) = \frac{(\Delta x)^2 (\Delta y)^2 \rho(i,\, j)}{2\varepsilon\left[(\Delta x)^2 + (\Delta y)^2\right]} +$$

$$\frac{(\Delta y)^2 \left[\varphi(i-1,\, j) + \varphi(i+1,\, j)\right] + (\Delta x)^2 \left[\varphi(i,\, j-1) + \varphi(i,\, j+1)\right]}{2\left[(\Delta x)^2 + (\Delta y)^2\right]} \tag{3.11}$$

Allowing for spatially varying permittivity requires a different form of Poisson's equation.

$$\nabla \bullet \left[\varepsilon(i,\, j) \nabla \varphi(i,\, j)\right] = -\rho(i,\, j) \tag{3.12}$$

Applying the finite difference method to this form of Poisson's equations relies on the introduction of coefficients corresponding to the five-point stencil, illustrated in Fig. 14.

$$a = a(i,\, j) = \left[\varepsilon(i,\, j) + \varepsilon(i+1,\, j)\right] \Delta y / \Delta x \tag{3.13}$$

$$b = b(i,\, j) = \left[\varepsilon(i,\, j) + \varepsilon(i-1,\, j)\right] \Delta y / \Delta x \tag{3.14}$$

$$d = d(i,\, j) = \left[\varepsilon(i,\, j) + \varepsilon(i,\, j+1)\right] \Delta x / \Delta y \tag{3.15}$$

$$e = e(i,\, j) = \left[\varepsilon(i,\, j) + \varepsilon(i,\, j-1)\right] \Delta x / \Delta y \tag{3.16}$$

$$c = c(i,\, j) = -\left[a(i,\, j) + b(i,\, j) + d(i,\, j) + e(i,\, j)\right] \tag{3.17}$$

The potential under this discretization scheme is:

$$\varphi(i,j)=\frac{1}{c}\left[a\varphi(i+1,j)+b\varphi(i-1,j)+d\varphi(i,j+1)+e\varphi(i,j-1)+\rho(i,j)\right] \tag{3.18}$$

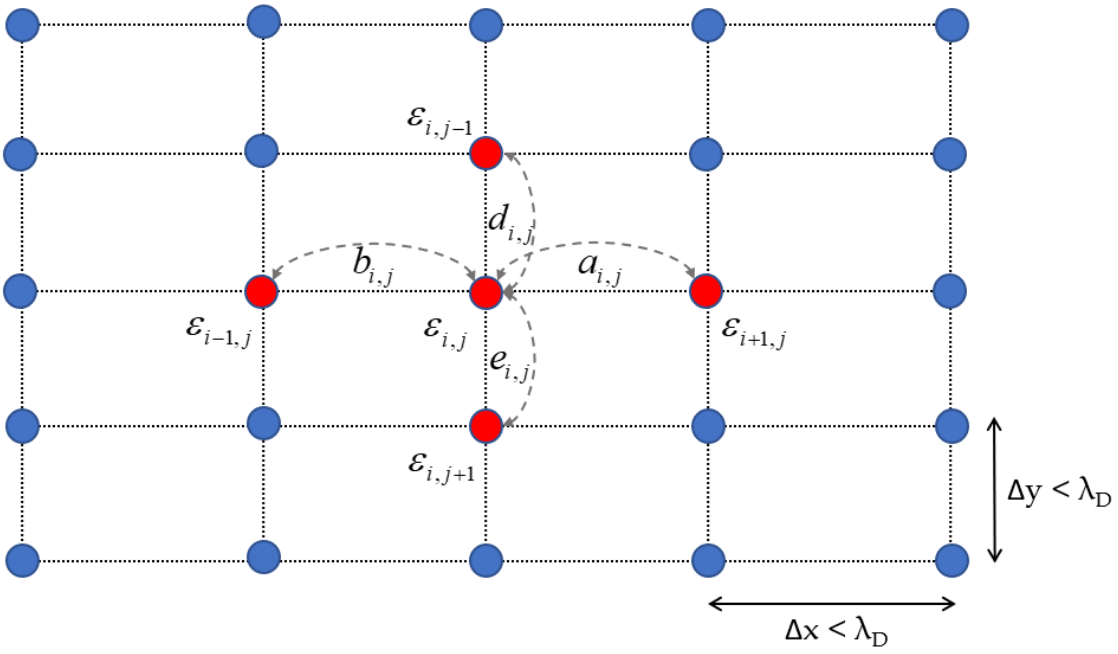

Figure 14 - Five-Point Stencil with Spatially Varying Permitivity: Indices i and j allow for the identification of each node within the mesh. This figure shows the spatially varying permittivity, $\varepsilon_{i,j}$, and coefficients as they relate to the central and adjacent nodes.

3.3 Calculating the Electric Field

Solving Poisson's equation for the electro-static potential throughout the device provides a means to determine the electric field; this electric filed acts as the driving force behind carrier transport in micro-electronic devices. Any given particle within the Monte Carlo ensemble can be located within the device structure, and the force on that particle can be calculated according to the potential at the surrounding nodes. While electric

potential has been calculated at each node point, the electric field and by extension the force on each ensemble particle is calculated within the cells.

$$\mathbf{F} = q\mathbf{E} \qquad \mathbf{E} = -\nabla\varphi \tag{3.19}$$

Discretizing along the 2-D mesh space defined for this simulation gives this form.

$$\boldsymbol{E}_{i,j}(x,y) = \frac{(\varphi_{i,j} - \varphi_{i+1,j}) + (\varphi_{i,j+1} - \varphi_{i+1,j+1})}{2\Delta x}, \frac{(\varphi_{i,j} - \varphi_{i,j+1}) + (\varphi_{i+1,j} - \varphi_{i+1,j+1})}{2\Delta y} \tag{3.20}$$

Figure 15 shows an illustration of the electric field calculation.

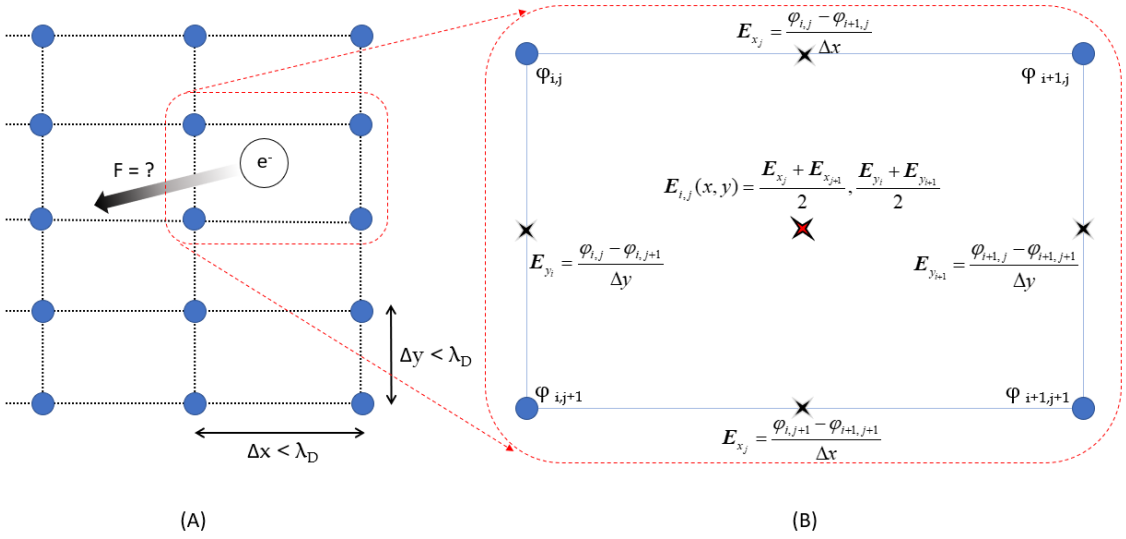

Figure 15 - Electron Field Calculation: An ensemble particle is located within the device mesh (A); the force on the particle is determined by calculating the electric field (B).

With the electric field is evaluated the free-flight/scatter procedure of the Monte Carlo solution to the Boltzmann transport equation (BTE) proceeds as before. The electric field parameter in the bulk Monte Carlo becomes a spatially varying quantity evaluated at each time step.

3.4 Particle Mesh Coupling

At the end of each time step in the simulation, after the carrier free-flight/scatter outcomes are calculated, Poisson's equation is solved. To account for the ensemble particles' contribution to the charge distribution, it is necessary to couple their charge with the device mesh. This coupling is achieved using a nearest element center (NEC) scheme, illustrated in Fig. 16. The charge of each ensemble particle has its charge distributed evenly amongst the mesh nodes surrounding the cell it occupies; this prevents self-force [31].

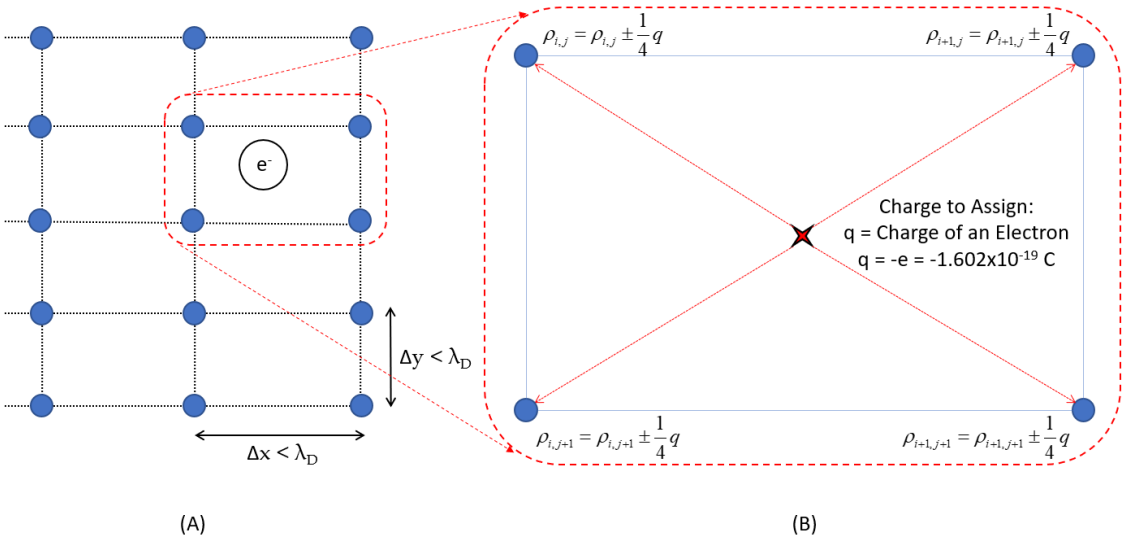

Figure 16 - Particle Mesh Coupling: An ensemble particle is located within the device mesh (A); the charge on this particle is assigned to the surrounding nodes (B). Charge assignment is repeated for each particle in the ensemble.

3.5 Boundary Conditions

Boundary conditions state how a numerical solution should behave at boundary nodes. In a Monte Carlo device solver, boundary conditions determine how external dynamics influence the solution of Poisson's equation. With transport inside the device structure described, what remains is to describe boundary conditions at the edge of the

simulation region. Particle-based device simulators use two types of boundary conditions which suit both the numerical methods used as well as the physical behavior of the device. Dirichlet boundary conditions are used at metal contacts and Neumann boundary conditions are used elsewhere.

Dirichlet boundary conditions are first order. In the context of the Poisson solver, a Dirichlet condition describes the *value* of the potential. Applying this condition at the contact nodes fits with physical intuition because typical operation of such devices includes applying a voltage to the contacts. The applied voltage results in an imposed electrical potential at the boundary nodes; thus, Poisson's equation has its solution fixed at these nodes.

Neumann boundary conditions are second order. A Neumann condition describes the *rate of change* instead of the *value* in the numerical solution. Applying this condition at the non-contact device boundary nodes fits with physical intuition because such devices are electrically isolated; therefore, there should be no flow of current at the device boundaries. No flow of current implies no charge flux; thus, Poisson's equation can be solved by setting the derivative of the charge density equal to zero at these nodes.

Boundary conditions also impose a specific behavior regarding the Monte Carlo ensemble. Contact nodes act as "active" boundaries. When applying a voltage at the contacts, it is possible for current to flow in the device. Ensemble particles, electrons or holes, can escape the simulation boundaries at the contacts. Similarly, ensemble particles can be injected or extracted at the contacts as needed to maintain charge neutrality at the contacts, thereby emulating the behavior of a perfect ohmic contact.

In contrast, the non-contact boundary nodes are “passive”. Since no current flows at non-contact boundaries, ensemble particles are reflected. Reflection can be specular, where the angle of reflection equals the angle of incidence; or diffuse, where the angle of reflection is random. In most regions of the device, it is enough to allow for specular reflection. Ensemble particles experience frequent scattering such that any given particles trajectory is constantly changing. In the channel region, diffuse or partially diffuse reflections at the gate boundary emulate the effects of surface roughness scattering.

3.6 Device Simulator Program Flow

The program flow of a particle-based device simulator incorporates the functional components described above. While some of the routines are specific to one device structure, others are generalized and can be used for alternative device structures with little to no modification. A carefully designed device simulator is modular and quite flexible, allowing it to be used to study numerous phenomena. The program flow of the particle-based device solver developed in this dissertation is described below and shown in Fig. 17.

Material parameters are initialized: physical parameters of the semiconductor, oxide, and metal materials in the device are defined. The device mesh is initialized based on Debye length to ensure adequate resolution for the quasi-static approximation. Poisson’s equation is solved for equilibrium conditions (no applied voltage) beginning with an initial guess for the potential profile based on the doping profile. Ensemble particles are initialized based on the equilibrium distribution described by Poisson’s equation. The main loop of the program describes the transport of ensemble particles (free-flight/scatter), how these particles interact with the device mesh (particle mesh coupling), and how the resulting distribution affects the electrostatics of the system (non-equilibrium Poisson solver).

During every time step these processes are evaluated self consistently until the results converge. When the prescribed number of simulation time steps have elapsed, the loop ends, and results are collected.

Bulk characteristics are calculated by running the Monte Carlo simulation without coupling to a device mesh. The carrier free-flight/scatter proceeds without the particle mesh coupling or the Poisson solver; electrostatic quantities such as the electric field are instead input to the program as parameters.

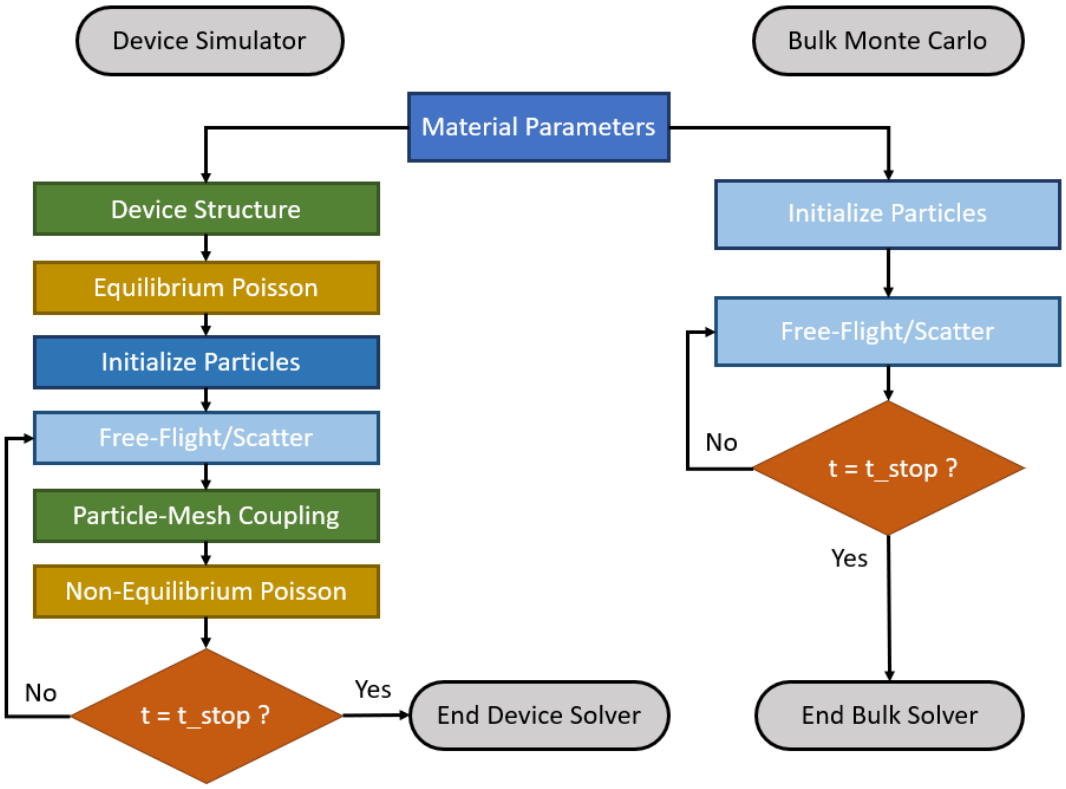

Figure 17 - Device Simulator Program Flow: The program flow illustrates the difference when solving for device behavior or bulk parameters.

3.7 Device Simulator Results

Observing device mesh quantities and ensemble particle attributes throughout the simulations gives significant insight into device behavior. Monitoring flux at the contacts allows for calculation of the current at the source and drain. In a typical MOSFET device,

the current in the source equals the current in the drain. Electric current is defined as the rate of flow of electric charge. If total number of charge carriers passing the source or drain contact is plotted versus time the current is proportional to the slope. Current is calculated by accounting for the charge of each ensemble particle (-e for electrons and +e for holes). Current in the source and drain is a good indicator of device performance. Analyzing the current under different bias conditions is a method of characterizing MOSFET devices. Cumulative charge and IV characteristics are shown for an NMOS device in Fig. 18 and for a PMOS device in Fig. 19.

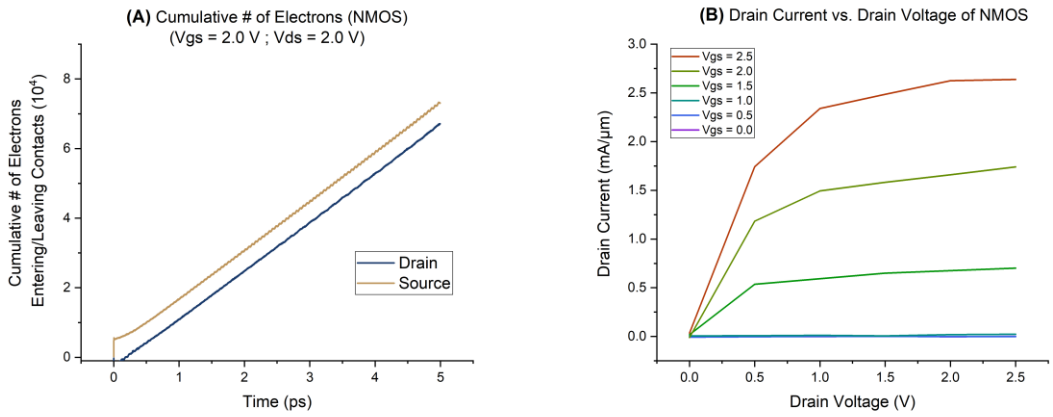

Figure 18 - NMOS Device Behavior: (A) Cumulative charge for an NMOS transistor. (B) Drain current versus drain voltage characteristics for a NMOS transistor.

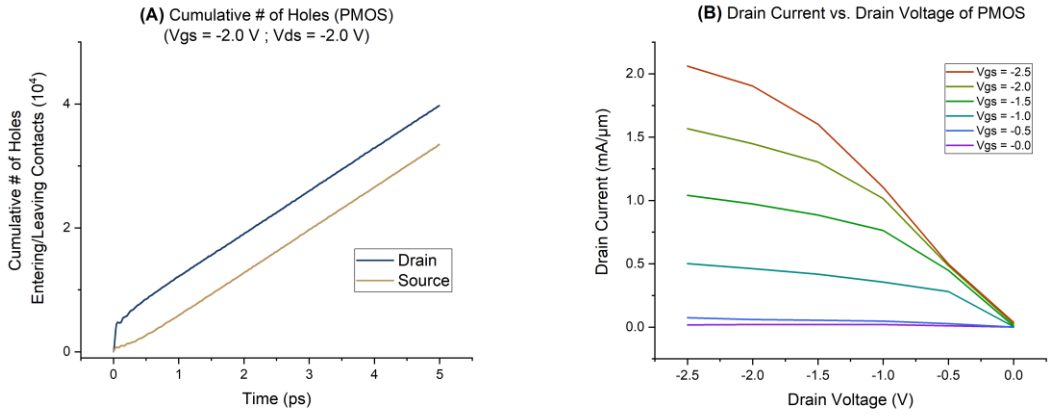

Figure 19 - PMOS Device Behavior: (A) Cumulative charge for an PMOS transistor. (B) Drain current versus drain voltage characteristics for a PMOS transistor.

CHAPTER 4

THERMAL TRANSPORT MODELING

4.1 Hot Carrier Effects

When highly energized electrons or holes, known as “hot carriers”, experience scattering, energy is released as lattice vibration in the form of acoustic or optical phonons. Acoustic phonons (E < 50meV) provide a mechanism for the dissipation of energy in the form of heat conduction. Optical phonons (E > 50meV) are highly localized lattice vibrations: they decay into acoustic phonons, then the energy is released as heat [32]. Thermal transport models describe these phenomena which are illustrated in Fig. 20. Modeling electron/phonon interactions at the device level and heat conduction at the macro scale provides a detailed picture of thermal characteristics in microelectronic devices and circuits.

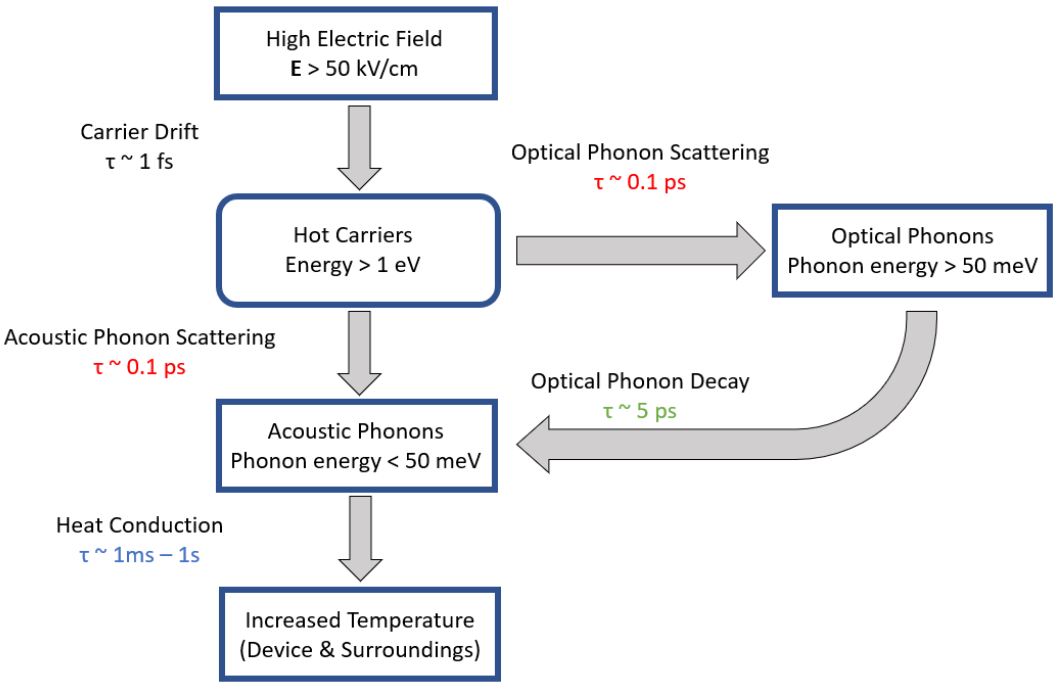

Figure 20 - Hot Carrier Effects: Energy is transferred from hot carriers to optical and acoustic phonons, allowing the energy to dissipate via heat conduction.

The significant difference in the duration of thermal processes in high field electronic devices necessitates the use of multi-scale modeling. The Monte Carlo based device simulator relies on the quasi-static approximation which requires a length scale on the order of the Debye length and a time scale on the order of the mean time between scattering events. The time scale determined by this criterion is appropriate for describing interactions between electrons and phonons, but it is orders of magnitude less than the time scale needed for heat conduction. A multiscale solution resolves this discrepancy by coupling the electron-phonon thermal transport model with the Monte Carlo device simulator, then solving for the heat conduction in the packaging and interconnects with a partially coupled Fourier law solver.

4.2 Thermal Transport Models

Many physical processes are affected by the transfer of thermal energy within a system. Thermal processes are dictated by the first law of thermodynamics: the change in energy (dE) of a system (which equals the sum of the Internal energy U, the kinetic energy KE and the potential energy PE) is equal to the net amount of heat (Q) supplied to the system minus the net work (W) done by the system on its surroundings

$$\frac{dE}{dt} = \frac{d(U + KE + PE)}{dt} = \frac{dU}{dt} = \dot{Q} - \dot{W} . \qquad (4.1)$$

For our system the change in KE, PE and net work is zero. The total heat accumulated in the system includes the heat going into the system (Q_{in}) minus the heat going out of the system (Q_{out}) plus the heat generated internally (Q_{gen}). Thus

$$\Delta E = \Delta U = Q_{in} - Q_{out} + Q_{gen} = Q_{acc} . \qquad (4.2)$$

Consider a thin element of thickness Δx in a large plane wall. Assume the density of the wall is ρ, the specific heat is c and the area normal to the heat transfer is A. An energy balance on this thin element during small time interval Δt can be expressed as:

$$\begin{pmatrix}\text{rate of heat}\\ \text{conduction}\\ \text{at x}\end{pmatrix} - \begin{pmatrix}\text{rate of heat}\\ \text{conduction}\\ \text{at x+}\Delta\text{x}\end{pmatrix} + \begin{pmatrix}\text{rate of heat}\\ \text{generation}\\ \text{inside the}\\ \text{element}\end{pmatrix} = \begin{pmatrix}\text{rate of change}\\ \text{of energy}\\ \text{inside the}\\ \text{element}\end{pmatrix} \tag{4.3a}$$

or:

$$\dot{Q}_x - \dot{Q}_{x+\Delta x} + \dot{E}_{gen.element} = \frac{\Delta E_{element}}{\Delta t} \approx -\frac{\partial \dot{Q}_x}{\partial x} + \dot{E}_{gen.element}\,, \tag{4.3b}$$

where Q_x=Q_{in} and $Q_{x+\Delta x}$=Q_{out} and $E_{gen.element}$=Q_{gen}. The change in energy content is:

$$\Delta E_{element} = \rho c_p A \Delta x \left(T_{t+\Delta t} - T_t\right) \approx \rho c_p A \Delta x \Delta t \frac{\partial T}{\partial t} \tag{4.4}$$

where T is the temperature. From the heat transfer (denoting the thermal conductivity with k) one has:

$$\frac{\dot{Q}}{A} = \dot{q} = -k\frac{\partial T}{\partial x}\,. \tag{4.5}$$

Substituting Eq. (4.4) and Eq. (4.5) into Eq. (4.3b) leads to the heat conduction equation:

$$\frac{\partial}{\partial x}\left(k\frac{\partial T}{\partial x}\right) + \dot{E}_{gen.element} = \rho c_p \frac{\partial T}{\partial t} \tag{4.6}$$

which is a cornerstone equation for the analysis of self-heating effects in commercial TCAD tools.

4.2.1 Joule Heating

Semiconductor microelectronic devices are one such system where internal heat generation mechanisms play a roll. These devices operate with a voltage bias across two

or more contact terminals which result in electric fields and current flow. Semiconductors operate on the physical principle of conduction. In a metal, conduction occurs because valence electrons de-localize and become shared among the positively charged nuclei. In metals, the valence and conduction bands overlap, and the Fermi level is in the conduction band. In insulators, conduction is inhibited because there is a sufficiently wide gap between the conduction and valence bands; the energy required for an electron to reach the conduction band is such that the material will often break down before it conducts. In a semiconductor there is a gap between the conduction and valence bands, but it is sufficiently small, and the Fermi level is sufficiently close to the conduction band such that energized electrons can escape into the conduction band and move freely within the material.

Electrical conduction in the presence of an electric field results in current flow. Electrons in the conduction band are negatively charged and accelerate under the force of an electric field. In semiconductors, and similar phenomenon occurs when states in the valence band are not occupied by an electron. These empty states, called holes, are positively charged and act remarkably like physical particles. Holes also accelerate under the force of an electric field.

Predictably, acceleration of electrons and holes is finite. The carriers interact with their surroundings, emit energy, and change direction due to scattering. The emission of energy through scattering is expressed as a local increase in thermal energy known as carrier self-heating. Carrier self-heating occurs even in simple electrical systems where the movement of individual carriers is not even considered. In such a system the flow of electrical charge is considered in terms of voltage, current, and power rather than the

movement of individual particles. Thermal effects are described according to the Joule heating model, without considering the contribution of individual carriers.

The Joule heating model is one way to describe the process by which the flow of electric current produces heat. Joule's law relates the power (energy per unit time) converted from electrical energy to thermal energy with the current flow and the resistance:

$$P = IV = I^2R = V^2/R \tag{4.7}$$

Compact models evaluate the current and voltage values associated with electronic devices; Joule heating is calculated by treating the device as a resistor and evaluating the basic form of Joule's law. This form of Joule's law is sufficient for simple systems but must be generalized for systems with non-uniform conductivity and non-uniform current density. Another form of Joule's law allows for heating to be calculated locally by considering the differential power per unit volume (dP/dV) as a function of the current density (**J**) and the electric field strength (**E**). This form is derived by considering that the current density (J) is the current (i) over the area and the electric field strength is the voltage (v) over the length.

$$\frac{dP}{dV} = \frac{d}{dV}(iv) \qquad J = \frac{i}{Area} \qquad E = \frac{v}{length} \tag{4.8}$$

$$\frac{dP}{dV} = \mathbf{J} \bullet \mathbf{E} \tag{4.9}$$

4.2.2 Modeling Thermal Transport Using the **J**·**E** method

The only prerequisite for the **J**·**E** method is the ability to calculate current density and electric field. This is inherent in the study of charge transport, consequently any charge transport model can be coupled with the **J**·**E** method for evaluating thermal transport.

The decision of how and to what extent this coupling is implemented depends on the complexity of the system. In some cases, it is enough to forward-couple results from the electrical solver and solve for the thermal behavior separately. The electric field and current density profiles allow for the calculation of power per unit volume throughout a device; the resulting heat generation profile goes into the heat transfer equation and solving the Fourier law determines the temperature throughout the device.

In other cases, the effects of heating in the device are sufficient to change the electrical behavior of the device. The results of the thermal solver must be back-coupled to the electrical solver. The thermal profile in the device is calculated as in the forward-coupled case and is subsequently used to re-evaluate the electrical characteristics while considering the temperature dependence of critical parameters. The Fermi-Dirac distribution is temperature dependent; therefore, the intrinsic carrier concentration is temperature dependent. Drift-diffusion solvers often use a temperature dependent mobility model to improve the accuracy of the transport model. Monte Carlo solvers can use temperature dependent scattering tables when evaluating for charge transport. Self-consistently solving for charge transport and thermal transport in a device requires evaluating the variables that effect both the electrical characteristics and the temperature profile iteratively until the results from both models converge.

4.3 Energy Balance Modeling for Phonons with Electrons as Free carriers

To simulate systems which exhibit thermal non-equilibrium requires a model that allows a local temperature difference between charge carriers and the phonon modes they interact with. One such methodology uses the energy balance equations which describe the transfer of thermal energy between charge carriers, phonons and the crystal lattice. The

energy balance equations describe the thermal energy of each contributor as an associated temperature [13]. The energy balance equation for optical phonons is:

$$C_{LO}\frac{\partial T_{LO}}{\partial t}=\frac{3nk_B}{2}\left(\frac{T_e-T_{LO}}{\tau_{e-LO}}\right)+\frac{nm^*v_d^2}{2\tau_{e-LO}}-C_{LO}\left(\frac{T_{LO}-T_A}{\tau_{LO-A}}\right) \tag{4.10}$$

The energy balance equation for acoustic phonons is:

$$C_A\frac{\partial T_A}{\partial t}=\nabla\left(k_A\nabla T_A\right)+C_{LO}\left(\frac{T_{LO}-T_A}{\tau_{LO-A}}\right)+\frac{3nk_B}{2}\left(\frac{T_e-T_L}{\tau_{e-L}}\right) \tag{4.11}$$

Equations (4.10) and (4.11) include the following quantities:

C_{LO}: Optical phonon specific heat capacity (J/kg·K)

C_A: Acoustic phonon specific heat capacity (J/kg·K)

T_{LO}: Optical phonon temperature (K)

T_A: Acoustic phonon temperature (K)

T_L: Lattice temperature (K)

T_e: Electron temperature (K)

n: Electron concentration (m^{-3})

m^*: Electron effective mass (kg)

v_d: Electron drift velocity (m/s)

τ_{e-LO}: Coupling time constant for electrons with optical phonons (s)

τ_{e-L}: Coupling time constant for electrons with the lattice (s)

τ_{LO-A}: Coupling time constant for optical phonons with acoustic phonons (s)

k_B: Boltzmann constant (J/K)

k_A: Thermal conductivity of the material (W/m·K)

In the quasi-static approximation, the partial differential optical phonon temperature with respect to time is assumed zero and Eq. (4.10) becomes:

$$C_{LO}\left(\frac{T_{LO}-T_A}{\tau_{LO-A}}\right)=-\frac{3nk_B}{2}\frac{T_{LO}}{\tau_{e-LO}}+\frac{1}{\tau_{e-LO}}\left(\frac{3}{2}nk_BT_e+\frac{1}{2}nm^*v_d^2\right) \tag{4.12}$$

Equation 4.12 includes the thermal energy, drift energy and total energy of electrons.

$$E_{Thermal}=\frac{3}{2}nk_BT_e \qquad E_{Drift}=\frac{1}{2}nm^*v_d^2 \qquad E_{Total}=\frac{3}{2}nk_BT_e+\frac{1}{2}nm^*v_d^2$$

Substituting these terms, Eq. (4.12) becomes:

$$C_{LO}T_{LO}\frac{\tau_{e-LO}}{\tau_{LO-A}}-C_{LO}T_A\frac{\tau_{e-LO}}{\tau_{LO-A}}=-\frac{3}{2}nk_BT_{LO}+E_{tot} \tag{4.13}$$

Solving for the optical phonon temperature gives the following:

$$T_{LO}\left[C_{LO}\frac{\tau_{e-LO}}{\tau_{LO-A}}+\frac{3}{2}nk_B\right]=C_{LO}T_A\frac{\tau_{e-LO}}{\tau_{LO-A}}+E_{tot} \tag{4.14}$$

In the quasi-static approximation, the partial differential of acoustic phonon temperature with respect to time is assumed zero. When acoustic phonon scattering is elastic the final term goes to zero. The lattice temperature is estimated to be equivalent to the acoustic phonon temperature ($T_L = T_A$). Under these assumptions Eq. (4.11) becomes:

$$-\nabla\bullet\left(k_A\nabla T_A\right)=C_{LO}\left(\frac{T_{LO}-T_A}{\tau_{LO-A}}\right) \tag{4.15}$$

Combined with Eq. (4.12) this gives:

$$-\nabla\bullet\left(k_A\nabla T_A\right)=\frac{3nk_B(T_e-T_{LO})}{2\tau_{e-LO}}+\frac{nm^*v_d^2}{2\tau_{e-LO}} \tag{4.16}$$

Defining $-T_A=T'_A$, (4.16) becomes:

$$\nabla \bullet \left(k_A \nabla T_A ' \right) = \frac{3nk_B (T_e - T_{LO})}{2\tau_{e-LO}} + \frac{nm^* v_d^2}{2\tau_{e-LO}} \tag{4.17}$$

There are four temperature variables described in these equations: electron temperature (T_e), optical phonon temperature (T_{LO}), acoustic phonon temperature (T_A), and lattice temperature (T_L). There are also time constants relating the rate of energy transfer and specific heat capacities for each of the phonon modes. Finally, there are electrical characteristics which determine how energized charge carriers will contribute to the thermal profile: carrier concentration (n) and drift velocity (v_d).

There are challenges in coupling these energy balance equations with the results from a charge transport solver. The drift-diffusion model, which models transport according to continuum equations and describes the flow of charge in terms current density, is inherently incompatible with the energy balance equations. The Monte Carlo method, which tracks the attributes of each charge carrier in an ensemble – and can be easily modified to include carrier temperature as one such attribute – is well suited for coupling with the energy balance model.

4.3.1 Coupling Charge Transport and Energy Transport

Coupling the charge transport results from the Monte Carlo solver to the energy balance equations requires evaluating the relevant electrical characteristics throughout the device. The energy balance equations need these characteristics as spatially varying quantities, but the Monte Carlo device solver tracks them as ensemble attributes: the attributes of each charge carrier are recorded as that carrier moves about the device structure. To deliver the spatially varying characteristics to the energy balance equations,

the carriers must be located, and their attributes assigned to an appropriate real-space grid. One methodology to accomplish this is the particle-mesh coupling discussed in section 3.3.

Electrical characteristics (T_e, n, and v_d) are available from the Monte Carlo ensemble via particle-mesh coupling. Three temperature variables remaining: lattice temperature (T_L), acoustic phonon temperature (T_A), and longitudinal optical phonon temperature (T_{LO}). Assuming lattice temperature is equal to acoustic phonon temperature, as shown in Eq. (4.15), leaves us with a system of two differential equations and two unknowns. The optical energy balance equation, Eq. (4.14) has an analytical solution. The acoustic energy balance equation, Eq. (4.17), a second order equation, follows the same successive over-relaxation (SOR) approach as the Poisson's equation solver.

Using device simulator particle attributes as inputs to the energy balance equations results in an un-coupled solution. Coupling the electrical solver with the thermal model requires that the device simulator account for contributions from the thermal dynamics using temperature dependent scattering rates. In the bulk solver, temperature is an input parameter used to calculate the scattering tables. In the coupled electro-thermal solver, the temperature dependence of scattering rates accounts for the phonon temperatures from the energy balance equation. The exchange of information between the Monte Carlo solver and the energy balance solver is illustrated in Fig. 21.

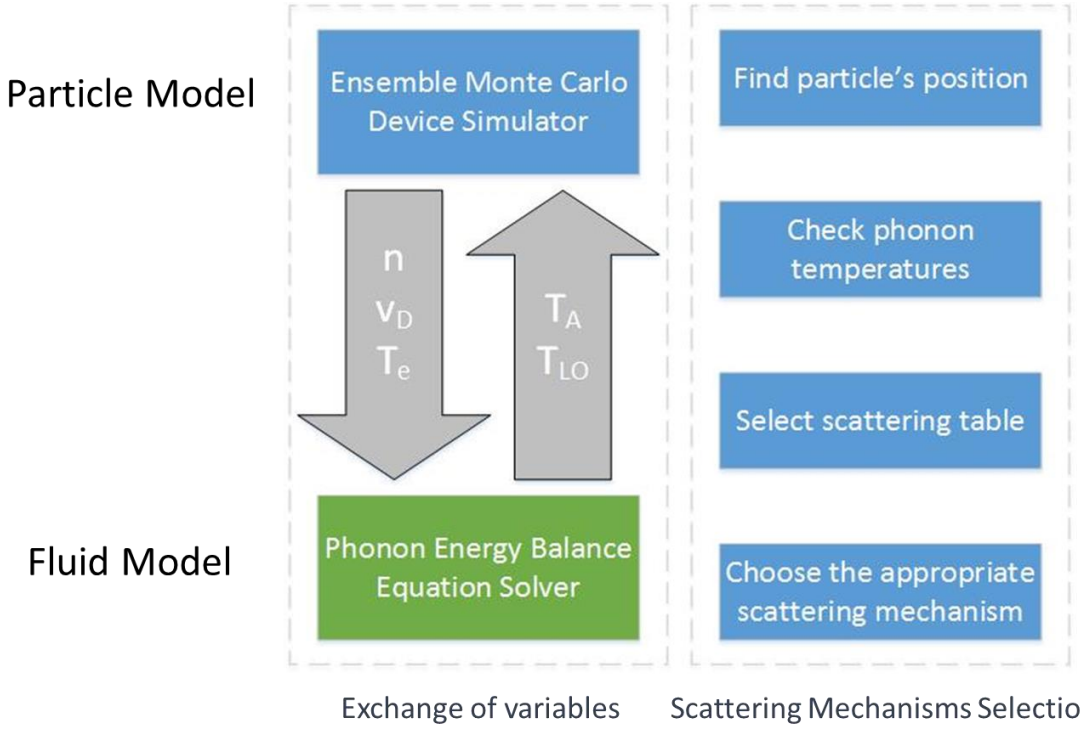

Figure 21 - Coupling the Electro-Thermal Solver: Particle attributes from the Monte Carlo device simulator, electron density, average velocity, and temperature, contribute to solution of the energy balance equation. The thermal profile from the energy balance equation influences the scattering mechanics of electrons in the Monte Carlo.

4.4 Electro-Thermal Solver Program Flow

The program flow of the electro-thermal device solver developed in this dissertation is described below and illustrated in Fig 22. The material parameter initialization includes thermal parameters in addition to electrostatic parameters. Updated material parameters are mapped to the device mesh according to the same criteria. Temperature dependence does not influence the solution to the Poisson equation; the equilibrium solution to the Poisson equation initializes the charge distribution for the Monte Carlo ensemble. The Monte Carlo method now includes optical and acoustic phonon temperatures; the first iteration of the Monte Carlo free-flight/scatter routine requires some initial guess for these temperatures. For simplicity, the initial free-flight/scatter uses room temperature scattering rates;

subsequent iterations use scattering rates based on the phonon temperatures from the energy balance equation. When the electrical solver reaches steady state, the thermal solver takes the electrostatic quantities (carrier density, carrier energy, and average velocity) and solves for acoustic and optical phonon temperatures. The energy balance equation requires a thermal boundary condition for the solution to converge. In the isolated device simulator, assuming room temperature at the edge of the device provides this boundary condition.

The energy balance equation, like Poisson's equation, is a second order partial differential equation. The numerical solution for the energy balance follows the same methodology as Poisson's equation. Linearizing and discretizing across a five-point stencil, shown in Fig. 13 and 14, facilitates the numerical solution. Generalization of the equation accounts for spatially varying thermal conductivity; this is analogous to spatially varying electric permittivity in the electrostatic equations. Solving iteratively using the successive over relaxation (SOR) method provides a converging result for the optical and acoustic phonon temperatures. When the solution of the energy balance equations reaches steady state, the phonon temperatures throughout the device structure are available for subsequent iterations of the Monte Carlo solver. With the temperature dependent scattering rates used in the electro-thermal solver, the effects of carrier self-heating influence electrical performance of the device.

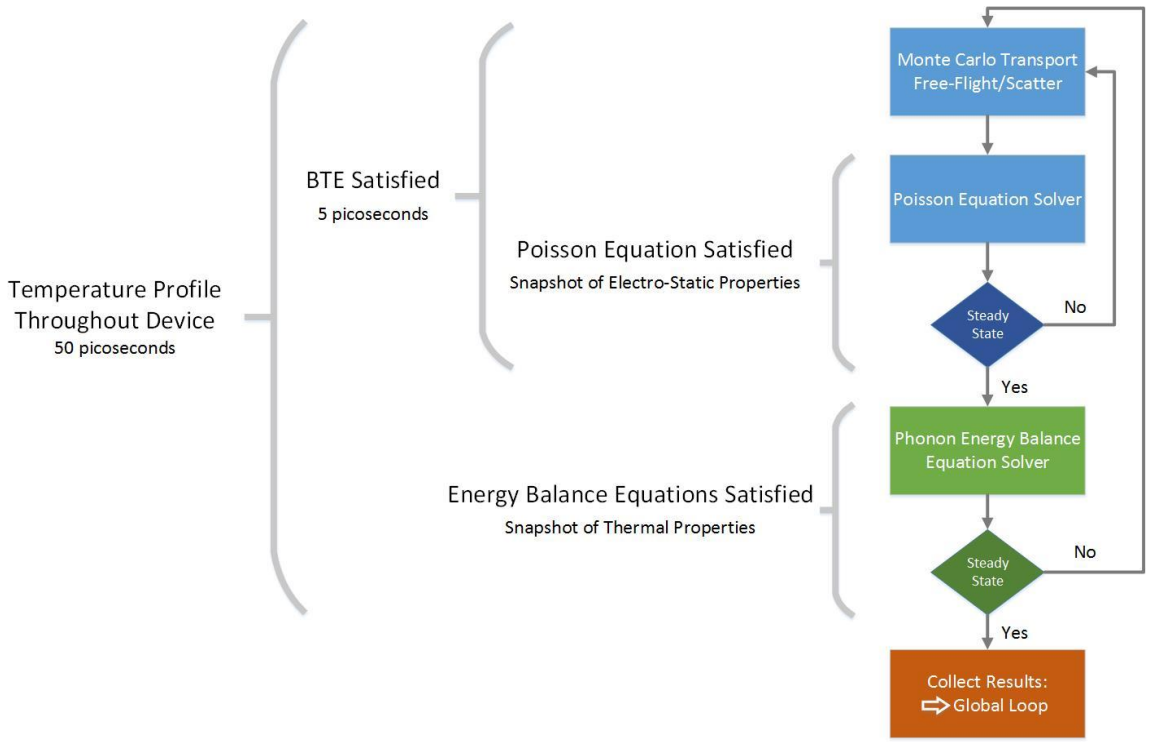

Figure 22 - Electro-Thermal Device Simulator Program Flow: This diagram shows the nested loop arrangement of the electrical and thermal portions of the solver. Results are collected when both parts reach steady state.

CHAPTER 5

MULTI-SCALE MODELING AND EXPERIMENTAL METHOD

5.1 Thermal Transport at the Macro Scale

In the coupled electro-thermal solver for an isolated device, boundary conditions assume room temperature at the edge of the device. This assumption is unrealistic in most semiconductor and microelectronics applications. On a chip, adjacent devices, isolating oxides, and conductive interconnects surround each device. Thermal transport in microelectronic devices is a complex process involving the surrounding materials in addition to the devices themselves. Discrepancies in time and length scales for device level transport and macro scale thermal transport necessitates multiscale modeling to study these phenomena.

Treating the microelectronic device as a heat source allows for the addition of a generation term when evaluating Fourier's law for thermal transport in the surrounding materials. The initial iteration assumes the device and its surroundings are at room temperature and the system is in equilibrium. Evaluating Fourier's law in the interconnects provides temperature boundary conditions for the device simulator. The electro-thermal device simulator reveals the phonon temperatures throughout the device. The lattice temperature is assumed equal to the acoustic phonon temperature, and this thermal profile determines the generation terms in subsequent iterations of the Fourier law solver.

With the device acting as a heat source in the macro-scale simulation region, the system is no longer in equilibrium. A positive heat flux is observed from the device towards the edge of the simulation region through the surrounding isolating oxide and conductive interconnects. Thermal conductivity can vary widely in the materials used in

microelectronic circuits; the dynamics of the system can vary depending on materials used and topology. This multiscale solution accounts for these dynamics. The results of the Fourier law solution for the macro-scale system provide more realistic temperature boundary conditions for the device simulator in subsequent iterations. The program flow, shown in Fig. 23, illustrates the coupling of the electro-thermal Monte Carlo device solver and the Fourie law interconnect solver.

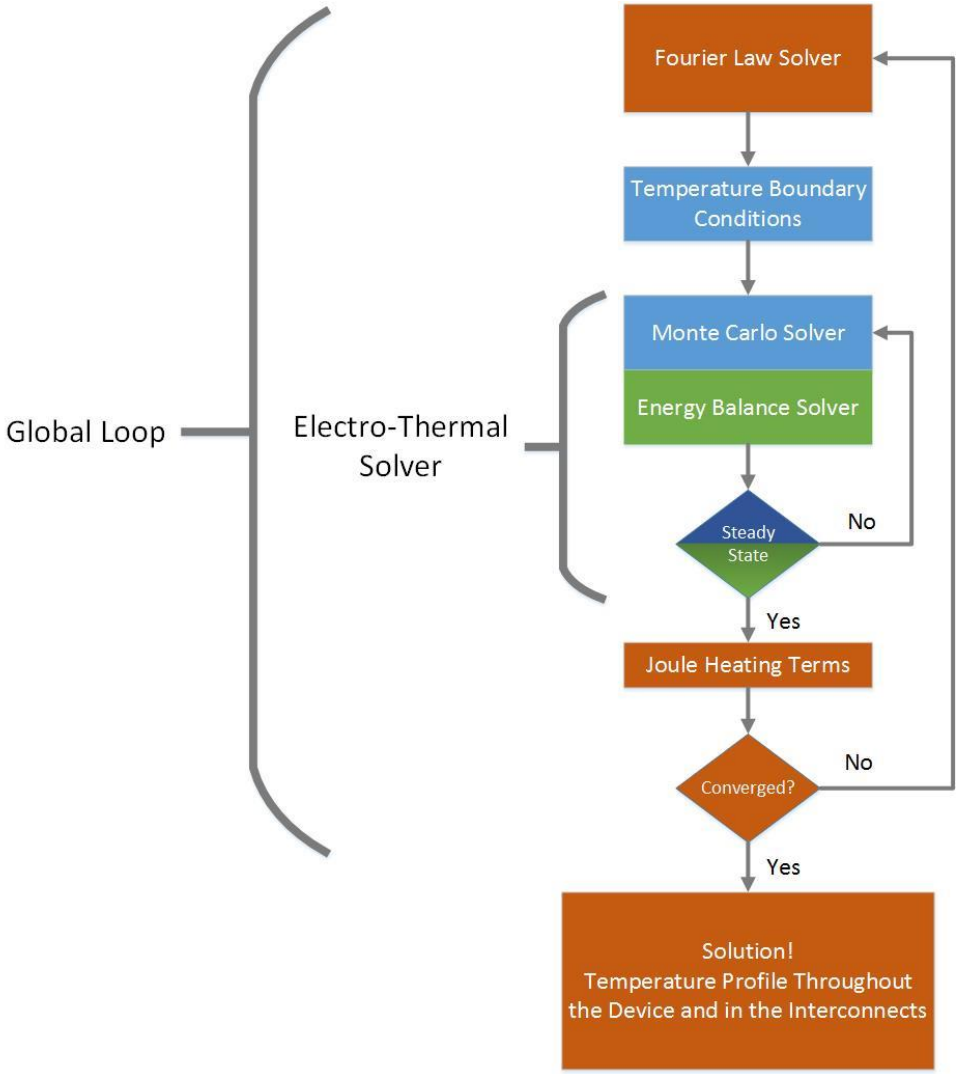

Figure 23 - Global Solver Program Flow: Results from the electro-thermal solver become inputs to the macro scale Fourier law solver; results from the Fourier law solver become boundary values in the electro-thermal solver.

5.2 Experimental Methods and Simulation of Temperature Sensing

Traditional methods of temperature sensing are often incompatible with semiconductor devices and microelectronic devices. Contact-reliant methods are likely to damage the structure rendering the results unusable.

5.2.1 Thermoreflectance Method

The thermoreflectance method is effective for the direct measurement of surface temperature in semiconductors and often used for studying thermal effects in devices. One downside to this method is that it is ineffective in sensing localized sub-surface effects. Careful study of the device theory and simulation of thermal effects in microelectronics suggest the formation of localized regions of increased temperature ("hot-spots") due to high electric fields and thermalization of the resulting high-energy electrons.

5.2.2 Heater-Sensor Method

Experimental researchers at Interuniversitair Micro-Electronica Centrum (IMEC) proposed a method of determining the temperature within a transistor in saturation by using an adjacent transistor in sub-threshold as a sensor. This experimental approach is directly comparable to simulation provided an identical device structure is simulated [33].

The IMEC method uses the temperature dependence of the sub-threshold slope of enhancement mode devices to determine the temperature in the structure. With a MOSFET device biased in the subthreshold region, the slope of the I-V curve indicates the temperature of the device's surroundings. To observe the self-heating process in active MOSFET devices, a subthreshold (sensor) device is placed adjacent to an active (heater) device, as shown in Fig. 24. The carrier self-heating in the active device causes a "hot-

spot" to form. Thermal transport in the semiconductor material causes the sub-threshold device to experience a proportional increased temperature.

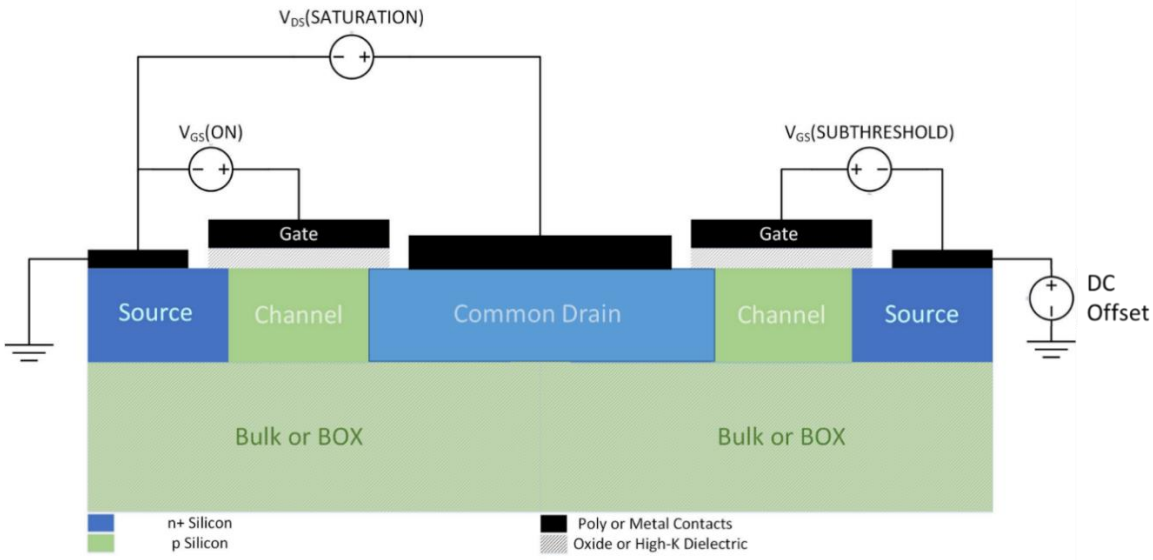

Figure 24 - Heater-Sensor Device Structure: this device structure illustrates the configuration of the heater (left) and sensor (right) devices.

The subthreshold sensor device is calibrated by directly heating the substrate on a hot plate and measuring the subthreshold I-V curve slope as a function of temperature. The subthreshold slope of the sensor device is again measured while actively biasing the heater device. As a hot spot forms in the heater device, the temperature in the sensor device is calculated as a function of the subthreshold slope based on the hot plate calibration. While this method does not provide a direct measurement of the temperature profile in the active device, it has one clear advantage: the entire experimental procedure can be simulated. Simulating both the heater and sensor devices allows for direct comparison with the experimental results. Comparing simulated I-V characteristics of the active device with the experimental I-V characteristics, shown in Fig. 25(a), verifies the accuracy of the electrical

modeling. Comparing the simulated sensor temperature with the experimental sensor temperature, shown in Fig. 25(b), verifies the accuracy of the thermal modeling.

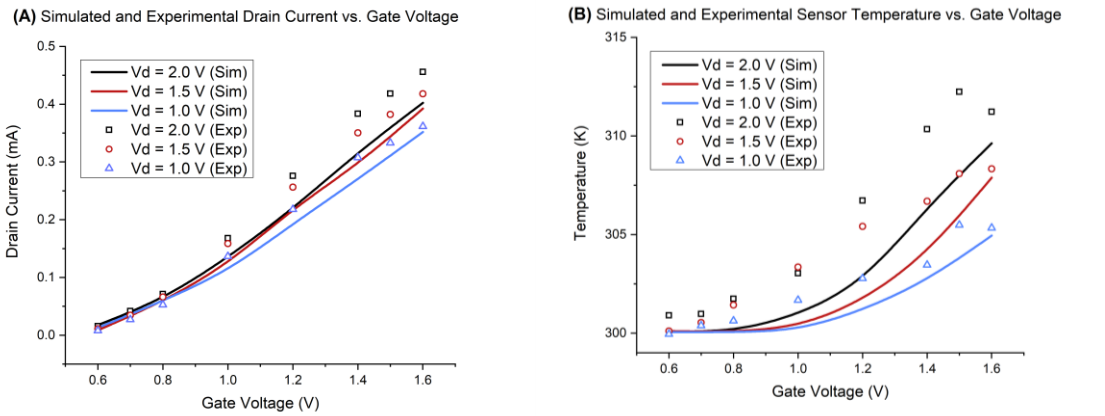

Figure 25 - Heater-Sensor Experiment and Simulation Results: (A) heater device I-V characteristics and (B) corresponding sensor device temperature. Experimental data provided courtesy of IMEC.

5.2.3 Simulated Temperature Profile Feasibility

The strategy of comparing simulated and experimental results for both electrical and thermal characteristics provides a strong framework for evaluating the feasability of the methodologies. The experimentatal method provides an opportunity for calibration of the temperature sensing and direct measurement of the electrical characteristcs, but offers limited insight for the underlying transport mechanisms. The simulation method directly models electro-thermal transport, offering exceptional insight into the location and nature of the "hot-spot", but it requires experimental validation. Verifying these results suggests the heator-sensor experiment actually measures self-heating, and the electro-thermal simulation provides an accurate thermal profile, as shown in Fig. 26. This approach provides a robust methodology for studying the nature and effects of carrier self-heating.

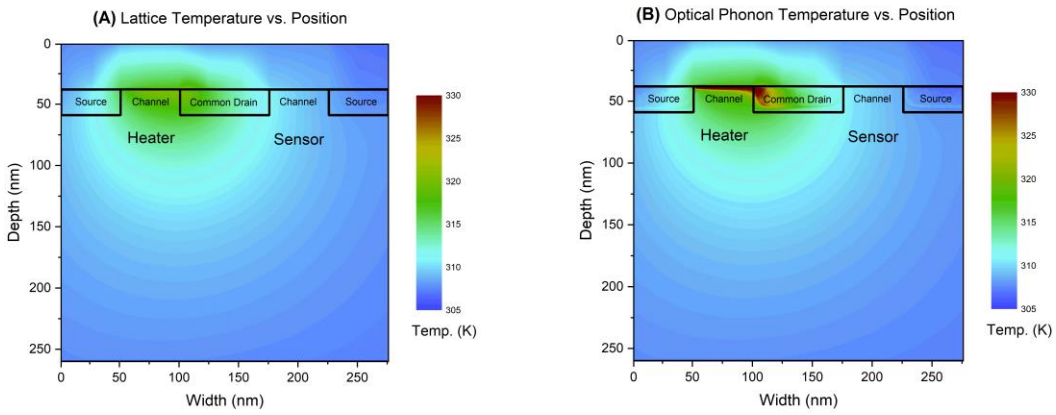

Figure 26 - Heater-Sensor Temperature Profiles: A localized hot spot forms in the drain region of the active device; this hot spot causes increased sensor device temperature resulting in a shift in the subthreshold slope. The lattice temperature profile (A) shows the increase in temperature and the optical phonon temperature profile (B) shows the pronounced hot spot in the drain of the active device.

The global device-interconnect simulator demonstrates the feasibility of multiscale modeling for studying the contributions of several concurrent phenomena. The Monte Carlo method solves for charge transport in the device, the coupled energy balance equations account for thermal interactions between charge carriers and phonons in the device, and the Fourier law evaluates for heat conduction outside the device. Comparisons with experimental results indicate this multiscale methodology goes beyond conceptualized behavior of a physical system to deliver simulated results which are comparable with measurable quantities. Expanding the capabilities of this methodology for CMOS simulations allows for the study of hot carrier effects in the context of micro-electronic circuit applications. This requires a charge transport model capable of evaluating for the motion of both electrons and holes, a device solver which can simulate both n-channel and p-channel MOSFETS (NMOS and PMOS), and a thermal transport model which accounts for the contribution of both hot electrons and hot hole effects. The

remainder of this dissertation details the development of a CMOS electro-thermal solver: the approach is as follows:

- Implement a Monte Carlo transport solver for holes
- Develop a device solver for PMOS devices
- Generalize the device solver for CMOS
- Verify the CMOS solver by studying circuit behavior (CMOS digital inverter)
- Couple the CMOS device solver with the energy balance thermal transport solver
- Verify the CMOS electro thermal solver

CHAPTER 6

CMOS DEVICE AND CIRCUIT SIMULATIONS

6.1 Methodology and Device Structure

To study the interactions between closely spaced microelectronic devices in analog and digital circuits, multiple devices need to be simulated. Since many integrated circuits, both analog and digital, are designed using complimentary devices (CMOS in the case of MOSFET based ICs) it is necessary to simulate electron and hole transport concurrently. In this dissertation, the Monte Carlo ensemble contains both electrons and holes. The transport is solved using the appropriate free-flight and scattering mechanisms and the Poisson solver accounts for contributions to the charge distribution from both carrier types. This allows for simulation of device behavior in the context of CMOS circuits, like the CMOS inverter shown in Fig. 27.

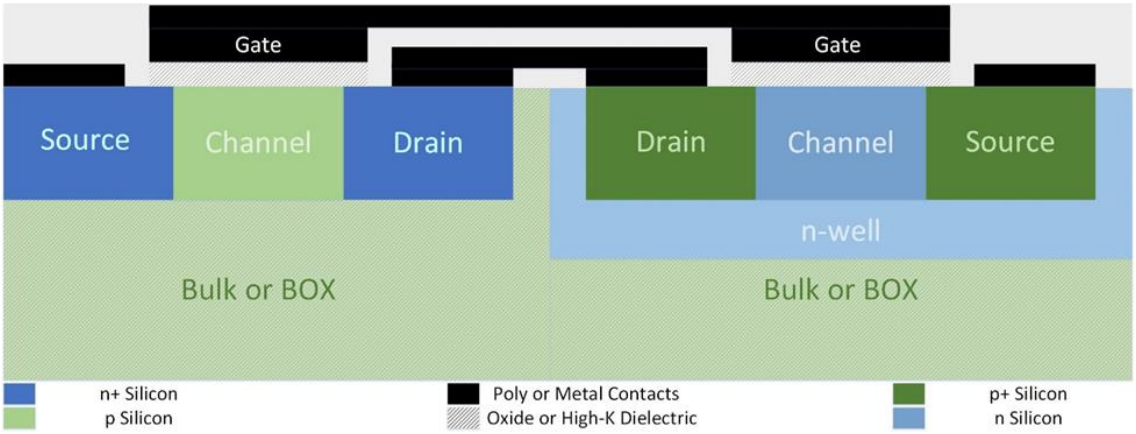

Figure 27 - CMOS Inverter Cross-Section: This is an illustration of the device structure used to demonstrate the dual-carrier methodology described in this dissertation.

For CMOS simulation, the Monte Carlo method includes both electrons and holes in the particle ensemble. Separate scattering tables for electrons and holes account for the difference in conduction and valence band structure. The Poisson solver accounts for the

contributions of electrons and holes to the charge distribution. Solving for NMOS and PMOS individually with the dual carrier method demonstrates the performance of the methodology and builds confidence moving forward to full CMOS simulations. I-V characteristics of individual NMOS and PMOS, simulated using the dual-carrier solver, are shown in Fig. 18 and 19.

6.2 Continuity Considerations

Full CMOS simulations also require a method to maintain continuity between series- and parallel-connected devices. For parallel connections, the voltage across the devices is equal, and the applied bias accounts for continuity. For series connections, such as in a CMOS inverter, current in the devices is equal, and the applied voltage cannot account for continuity. In a CMOS inverter the drain terminals of the NMOS and PMOS form the output. The voltage at the output depends on the behavior of the circuit. Output voltage is an emergent quantity rather than an applied quantity. Simulation of CMOS circuits requires a methodology to address this issue.

6.2.1 Fully Self Consistent Approach

In a fully self-consistent solution, input and supply terminals have an applied bias, whereas output terminals have modified boundary conditions consistent with the observed circuit behavior. A CMOS inverter consists of series connected NMOS and PMOS transistors with power supplied at the source terminals, the input applied to the gate terminals, and the output at the drain terminals. Self-consistency in this configuration requires drain boundary conditions that maintain current continuity in these series connected devices. Current continuity in the circuit is analogous to charge continuity in the device. Selective carrier injection and extraction at the drain terminal of each device is one

approach to maintain charge continuity. Charge extraction at the drain of the NMOS transistor results in charge injection at the drain of the PMOS transistor. Since this is a dual carrier model, several available options are equivalent in terms of charge continuity. For example, in the event of extraction of an electron at the drain of the NMOS, injection of an electron or extraction of a hole in the drain of the PMOS results in equivalent charge flux.

Should the charge continuity scheme use a 1:1 correspondence (electron-for-electron, hole-for-hole) or a majority carrier correspondence (electrons in the n-channel and holes in the p-channel)? Is it necessary to model the NMOS and PMOS as well as a resistive element such as a metal or polysilicon contact connecting the drain terminals? What happens to charge continuity when there is a capacitive element at the output, which charges and discharges as the inverter switches? It would be interesting to implement a fully self-consistent solution where output voltage is an emergent quantity dependent on the behavior of the circuit, but such a solution is not presented in this dissertation.

6.2.2 Parametric Iteration Approach

While slightly less elegant, another method of addressing the continuity issue is to manipulate bias conditions while applying a voltage at each terminal. Applying a voltage at the source, gate, and drain terminals of a MOSFET results in current flow in the channel. The drain current of a MOSFET is dependent on the bias conditions at the terminals; a unique set of applied voltages result in a specific drain current. In a CMOS inverter, the drain terminals of both NMOS and PMOS are series connected and act as the output of the logic circuit; therefore, no voltage bias is applied. Kirchhoff's first law states that the charge entering a node is exactly equal to the charge leaving the node; therefore, the drain currents of the NMOS and PMOS must be exactly equal. Given a set of input conditions, or voltage

biases on the gate and source terminals, there is only one value for the drain voltage that results in equal drain currents: the output voltage. Rather than maintaining current continuity through injection and extraction statistics, continuity is maintained by applying the correct output voltage.

6.3 Results

The correct output voltage is determined iteratively. For a set of input biases, the output is swept from 0V (ground) to 2.5V (supply or V_{DD}). By comparing the resulting drain currents of the NMOS and PMOS, shown in Fig. 28, the correct value of the output voltage is constrained. Iteration continues until the desired accuracy is achieved. The voltage transfer curve of the inverter, shown in Fig. 29, is constructed. Further simulations of the inverter need only select input and output values that correspond to the voltage transfer curve.

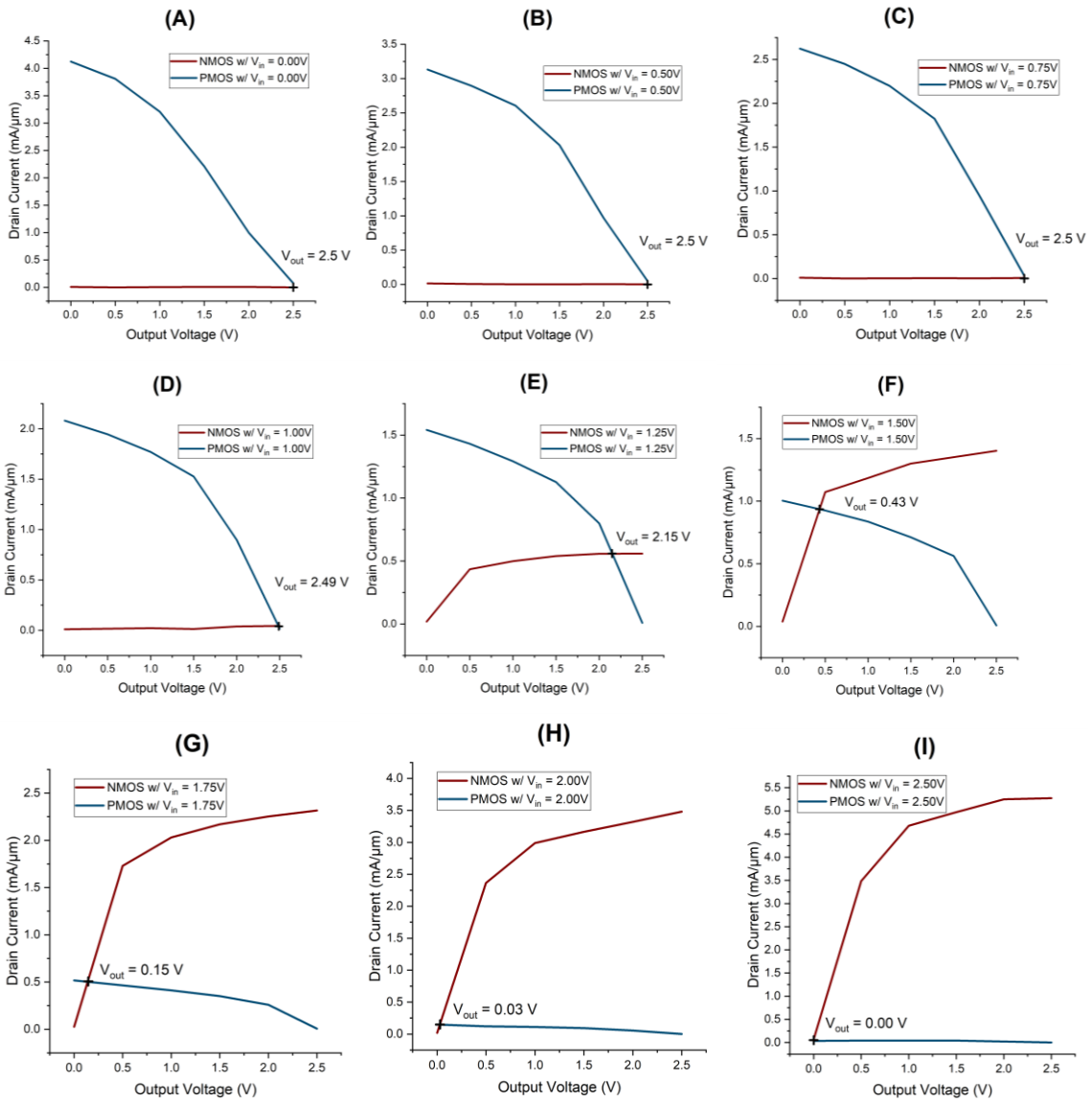

Figure 28 - Parametric Iteration Method: The I-V characteristics show the drain currents as a function of output voltage for a given input voltage: (A) V_{in} = 0V, (B) V_{in} = .5V, (C) V_{in} = .75V, (D) V_{in} = 1V, (E) V_{in} = 1.25V, (F) V_{in} = 1.5V, (G) V_{in} = 1.75V, (H) V_{in} = 2V, (I) V_{in} = 2.5V. Current continuity is satisfied when the correct output voltage is found and the NMOS and PMOS have equivalent drain current.

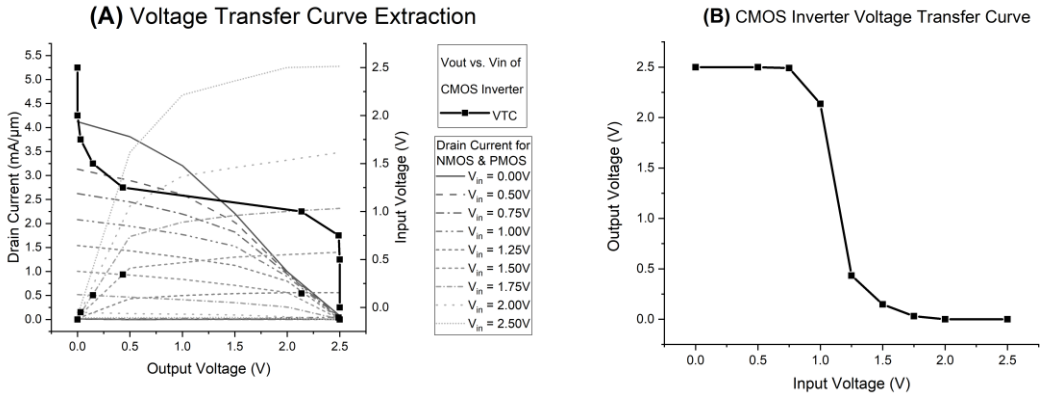

Figure 29 - Extracted Voltage Transfer Curve: These plots show the extraction methodology (A) and the resulting voltage transfer curve (B) of the CMOS inverter.

6.4 Discussion

Figures 28 and 29 show that the macro-scale behavior (current and voltage) of CMOS circuits can be modeled using the parametric iteration method described in section 6.2.2. This device level simulation, with carefully selected continuity conditions, accurately predicts the behavior of circuit. Coupling the CMOS device solver with the electro-thermal model from chapter 4 allows for the study device level thermal behavior within the context of CMOS microelectronic circuits.

CHAPTER 7

CMOS ELECTRO-THERMAL MODELING

7.1 Including Hole-Phonon Interaction to the Energy Balance Model

The dual carrier Monte Carlo device simulator can solve for electron and hole transport characteristics simultaneously. To solve for thermal transport requires the modification of the energy balance equations, Eq. (4.10) and (4.14), to account for the contribution of both electrons and holes.

The energy balance equation for optical phonons is:

$$C_{LO}\frac{\partial T_{LO}}{\partial t}=\frac{3nk_B}{2}\left(\frac{T_e-T_{LO}}{\tau_{e-LO}}\right)+\frac{3pk_B}{2}\left(\frac{T_h-T_{LO}}{\tau_{h-LO}}\right)+\frac{nm_e^*v_{de}^2}{2\tau_{e-LO}}+\frac{pm_h^*v_{dh}^2}{2\tau_{h-LO}}-C_{LO}\left(\frac{T_{LO}-T_A}{\tau_{LO-A}}\right) \quad (7.1)$$

The energy balance equation for acoustic phonons is:

$$C_A\frac{\partial T_A}{\partial t}=\nabla\left(k_A\nabla T_A\right)+C_{LO}\left(\frac{T_{LO}-T_A}{\tau_{LO-A}}\right)+\frac{3nk_B}{2}\left(\frac{T_e-T_L}{\tau_{e-L}}\right)+\frac{3pk_B}{2}\left(\frac{T_h-T_L}{\tau_{h-L}}\right) \quad (7.2)$$

Equations (7.1) and (7.2) include the following quantities:

C_{LO}: Optical phonon specific heat capacity (J/kg·K)

C_A: Acoustic phonon specific heat capacity (J/kg·K)

T_{LO}: Optical phonon temperature (K)

T_A: Acoustic phonon temperature (K)

T_L: Lattice temperature (K)

T_e: Electron temperature (K)

T_h: Hole temperature (K)

n: Electron concentration (m^{-3})

m_e^*: Electron effective mass (kg)

v_{de}: Electron drift velocity (m/s)

p: Hole concentration (m^{-3})

m_h^*: Hole effective mass (kg)

v_{dh}: Hole drift velocity (m/s)

τ_{e-LO}: Coupling time constant for electrons with optical phonons (s)

τ_{h-LO}: Coupling time constant for holes with optical phonons (s)

τ_{e-L}: Coupling time constant for electrons with the lattice (s)

τ_{h-L}: Coupling time constant for holes with the lattice (s)

τ_{LO-A}: Coupling time constant for optical phonons with acoustic phonons (s)

k_B: Boltzmann constant (J/K)

k_A: Thermal conductivity of the material (W/m·K)

Solving the optical energy balance equation under quasi-static approximation is shown in Eq. (4.11) - (4.15). Including holes in Eq. (4.12) gives the following:

$$C_{LO}\left(\frac{T_{LO}-T_A}{\tau_{LO-A}}\right)=-\frac{3nk_BT_{LO}}{2\tau_{e-LO}}-\frac{3pk_BT_{LO}}{2\tau_{h-LO}}+\frac{E_{total}^e}{\tau_{e-LO}}+\frac{E_{total}^h}{\tau_{h-LO}} \tag{7.3}$$

This dissertation assumes the relaxation time constants for electrons and holes are equal:

$$\tau_{e-LO}=\tau_{h-LO}=\tau_{eh-LO}$$

With this assumption, Eq. (7.3) reduces to:

$$C_{LO}T_{LO}\frac{\tau_{eh-LO}}{\tau_{LO-A}}-C_{LO}T_A\frac{\tau_{eh-LO}}{\tau_{LO-A}}=-\frac{3}{2}(n+p)k_BT_{LO}+E_{total}^e+E_{total}^h \tag{7.4}$$

Solving for the optical phonon temperature gives:

$$T_{LO}\left[C_{LO}\frac{\tau_{eh-LO}}{\tau_{LO-A}}+\frac{3}{2}(n+p)k_B\right]=C_{LO}T_A\frac{\tau_{eh-LO}}{\tau_{LO-A}}+E^{e}_{total}+E^{h}_{total} \tag{7.5}$$

Equations (4.14) - (4.17) solve the acoustic energy balance equation in the quasi-static approximation with elastic acoustic phonon scattering and lattice temperature assumed to equal acoustic phonon temperature. Including holes in Eq. (4.17) becomes:

$$\nabla\bullet\left(k_A\nabla T_A'\right)=\frac{3nk_B\left(T_e-T_{LO}\right)}{2\tau_{e-LO}}+\frac{3pk_B\left(T_h-T_{LO}\right)}{2\tau_{h-LO}}+\frac{nm_e^{*}v_{de}^{2}}{2\tau_{e-LO}}+\frac{pm_h^{*}v_{dh}^{2}}{2\tau_{h-LO}} \tag{7.6}$$

This dissertation assumes the relaxation time constants for electrons and holes are equal:

$$\tau_{e-LO}=\tau_{h-LO}=\tau_{eh-LO}$$

With this assumption, Eq. (7.6) reduces to:

$$\nabla\bullet\left(k_A\nabla T_A'\right)=\frac{3nk_B\left(T_e+T_h-T_{LO}\right)}{2\tau_{eh-LO}}+\frac{nm_e^{*}v_{de}^{2}+pm_h^{*}v_{dh}^{2}}{2\tau_{eh-LO}} \tag{7.7}$$

The optical energy balance equation, Eq. (7.5), has an analytical solution. The acoustic energy balance equation, Eq. (7.7), a second order partial differential equation, uses the same successive over-relaxation (SOR) approach as the Poisson's equation solver.

This system of equations requires electron and hole parameters from the electrical characterization. Some of the requisite parameters are readily available because they are used to evaluate charge transport behavior; others are calculated explicitly in the thermal transport solver. Particle attributes are stored as ensemble variables. The physical characteristics of each charge carrier are updated as it travels through the device. The thermal transport solver requires these attributes as spatial quantities. Individual ensemble particle attributes are mapped to real-space coordinates appropriately using the particle-

mesh coupling approach described in chapters 3 and 4. With the electron and hole characteristics from the Monte Carlo ensemble, the system of energy balance equations is solved for the optical and acoustic phonon temperatures. The result is a thermal transport modeling methodology which accounts for contributions from electron and hole hot carrier effects.

7.2 Device Structure Used in CMOS Simulations

The device structure is shown in Fig. 30. Charge and thermal transport are solved in 2-D.

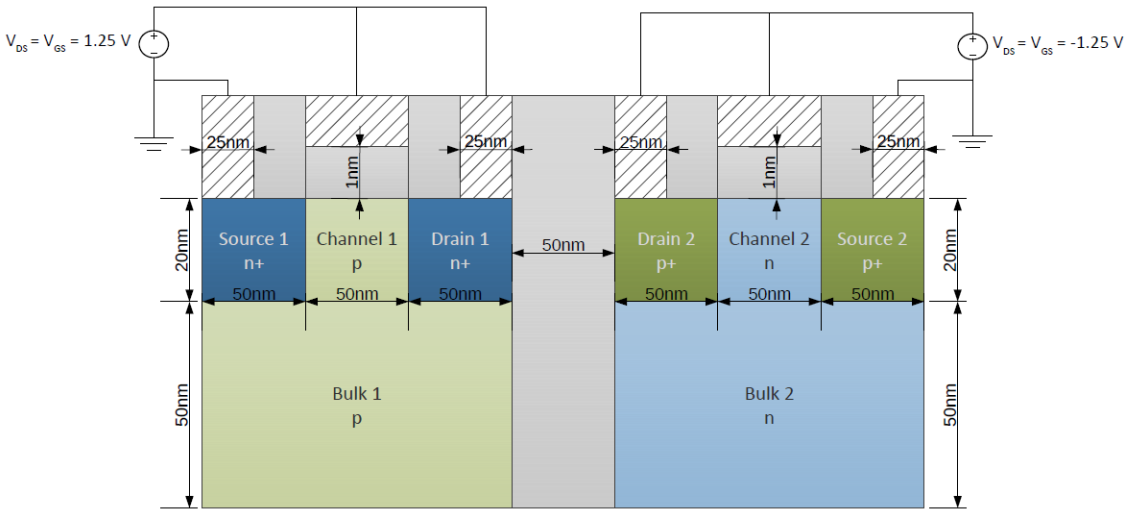

Figure 30 - CMOS Electro-Thermal Device Structure: NMOS and PMOS transisitors are biased in saturation (diode connected). This is the exact device structure used in CMOS electro-thermal simulations.

A list of key parameters and operating conditions is shown in Table 1.

Table 3: Device Geometry and Operating Parameters

Parameter	Value	
Device Width	5 µm	
Source, Drain, and Channel Length	50 nm	
Source and Drain Depth	20 nm	
Bulk Depth	50 nm	
Gate Oxide Thickness	1 nm	
Device Separation	50 nm	
Bias Voltage ($V_{GS} = V_{DS}$)	1.25 V (NMOS)	-1.25V (PMOS)

The Monte Carlo solver gives the velocity of electrons and holes, shown in terms of directional components in Fig. 31 and 32, and in terms of magnitude in Fig. 33.

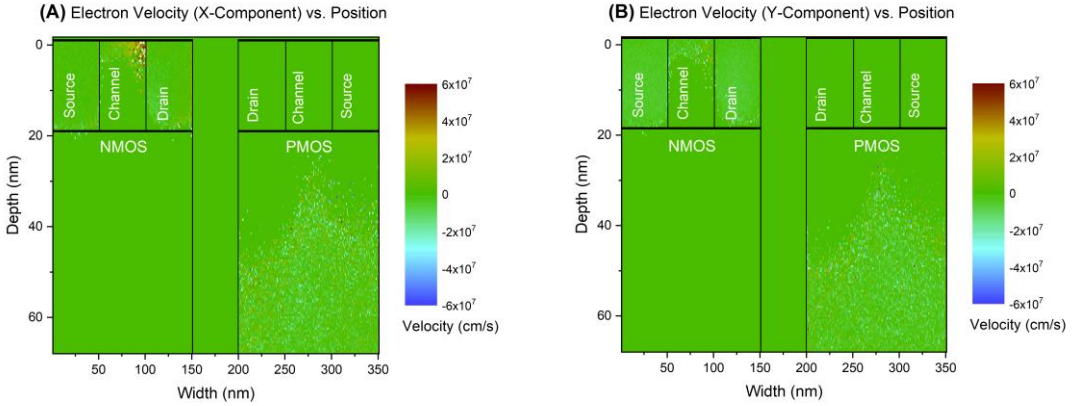

Figure 31 - Electron Component Velocity: The x-component (A) and y-component (B) of the electron velocity are mapped to the device structure.

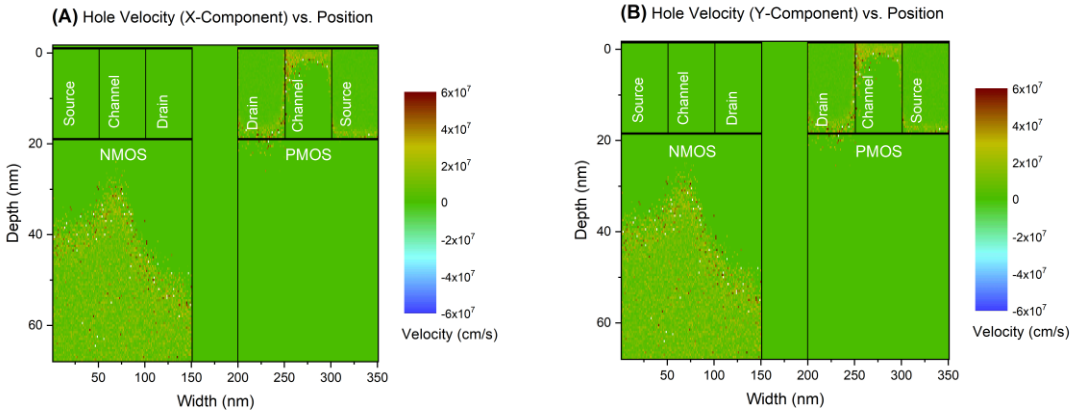

Figure 32 - Hole Component Velocity: The x-component (A) and y-component (B) of the hole velocity are mapped to the device structure.

The energy balance equations for thermal transport call for the drift velocity of charge carriers, shown in Fig. 33. The magnitude of the drift velocity is calculated by considering the contribution of the x- and y- component velocities.

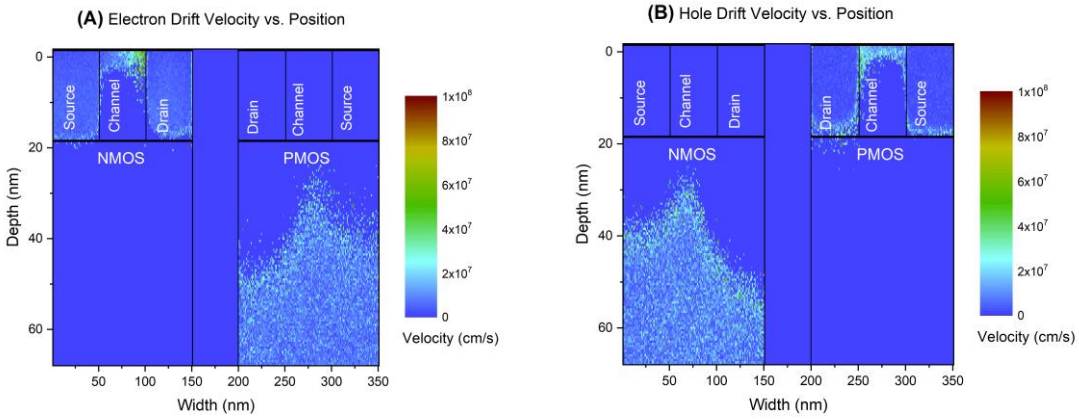

Figure 33 - Electron and Hole Drift Velocity: The electron drift velocity (A) and hole drift velocity (B) are mapped to the device structure.

In equations 7.5 and 7.7 carrier velocity appears in the form of a drift energy. The drift energy used in the thermal solver is calculated from the drift velocity. This energy is averaged until the Monte Carlo solver reaches steady state to reduces noise in the energy profile and help thermal solver converge. The average carrier drift energy, shown in Fig. 34, is used to evaluate thermal transport behavior.

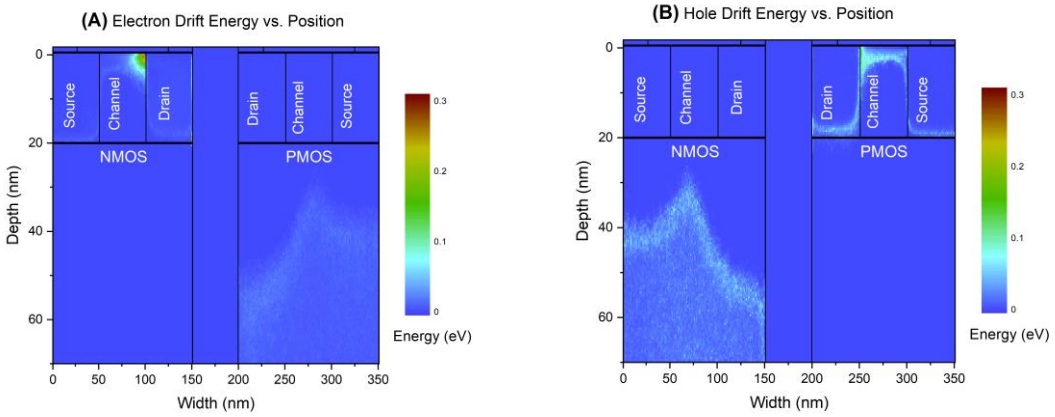

Figure 34 - Electron and Hole Drift Energy: The drift energy of electrons (A) and holes (B) are averaged until the Monte Carlo solver converges and mapped to the device structure.

The Monte Carlo solver also calculates the charge carrier thermal energy, shown in Fig. 35, needed to determine the rate and outcomes of scattering events in the free-flight/scatter segment of the device simulations.

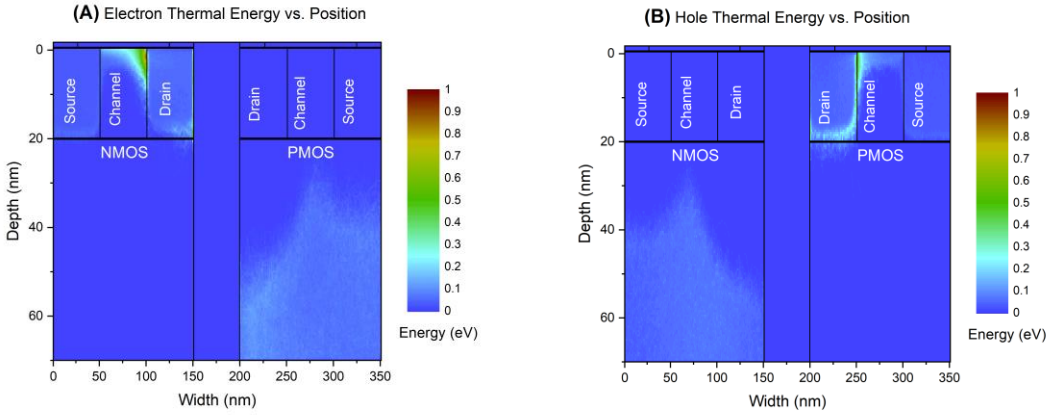

Figure 35 - Electron and Hole Thermal Energy: Electron thermal energy (A) and hole thermal energy (B) are calculated by the Monte Carlo solver, averaged until the Monte Carlo solver converges and mapped to the device structure.

The thermal energy is used to determine carrier temperature, shown in Fig. 36, which is needed to evaluate Eq. 7.7.

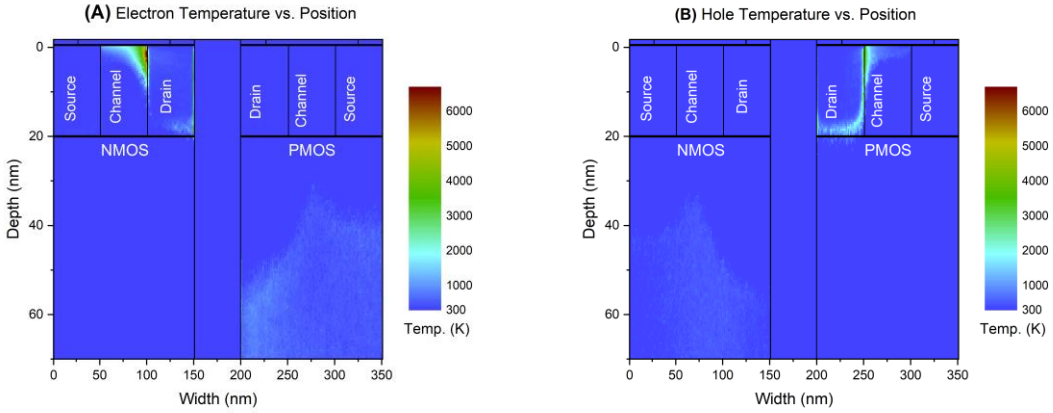

Figure 36 - Electron and Hole Temperature: Electron temperature (A) and hole temperature (B) are calculated from the thermal energy. Because the thermal energy is averaged, the calculated temperature also has reduced random noise.

The total electron and hole energy needed to evaluate Eq. 7.5 are calculated as the sum of drift energy and thermal energy. Figure 37 shows the total energy profile.

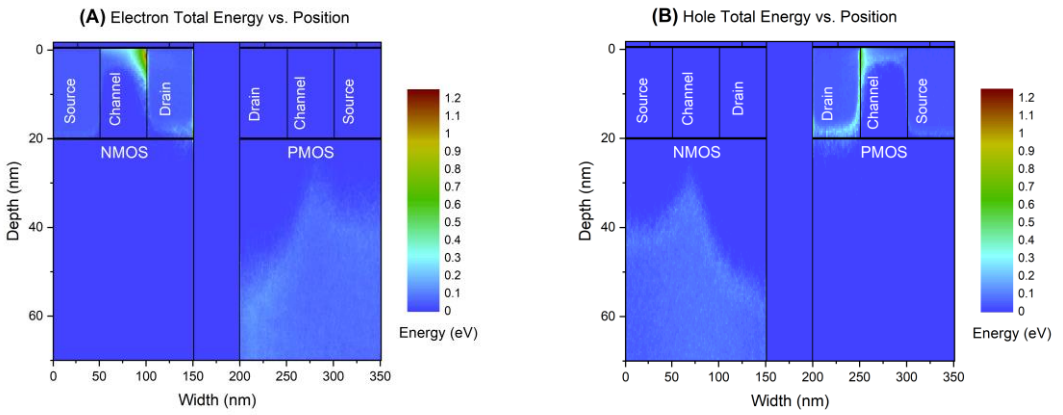

Figure 37 - Electron and Hole Total Energy: Total energy of electrons (A) and holes (B) is calculated as the sum of the drift energy and thermal energy.

Carrier density throughout the device is calculated using the nearest element center (NEC) charge assignment scheme. The carrier density, shown in Fig. 38, is used in Eq. 7.5 and 7.7 to calculate the weight of the electron and hole contribution to the phonon energy balance.

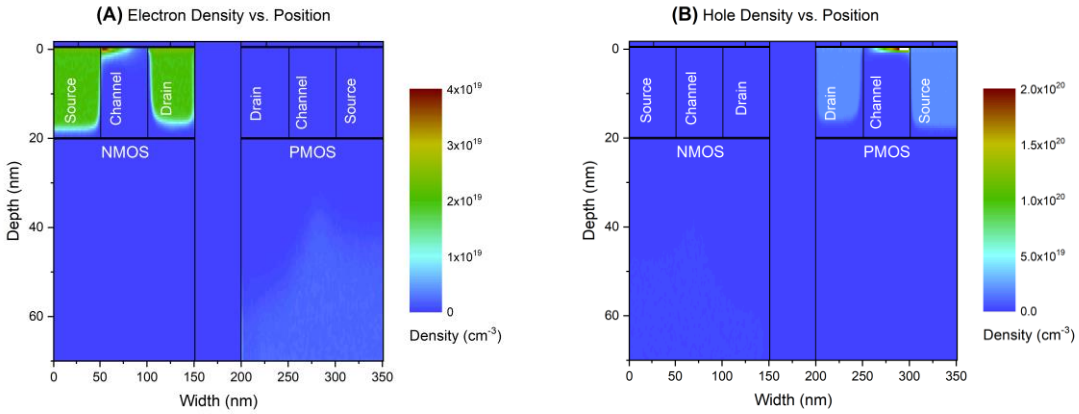

Figure 38 - Electron and Hole Density: Electron density (A) and hole density (B) are calculated by NEC scheme in the Monte Carlo solver.

7.3 Combined Electron and Hole Device Characteristics

To understand the contributions to the thermal behavior from hot electrons and hot holes carrier attributes are examined as a whole: electrons with holes. Average carrier drift

velocity is calculated by aggregating the velocity of electrons and holes and weighting by their respective densities, effectively combining the profiles from Fig. 33. Figure 39 shows that the drift velocity profiles of the NMOS and PMOS differ due to the differences in charge transport dynamics of electrons and holes.

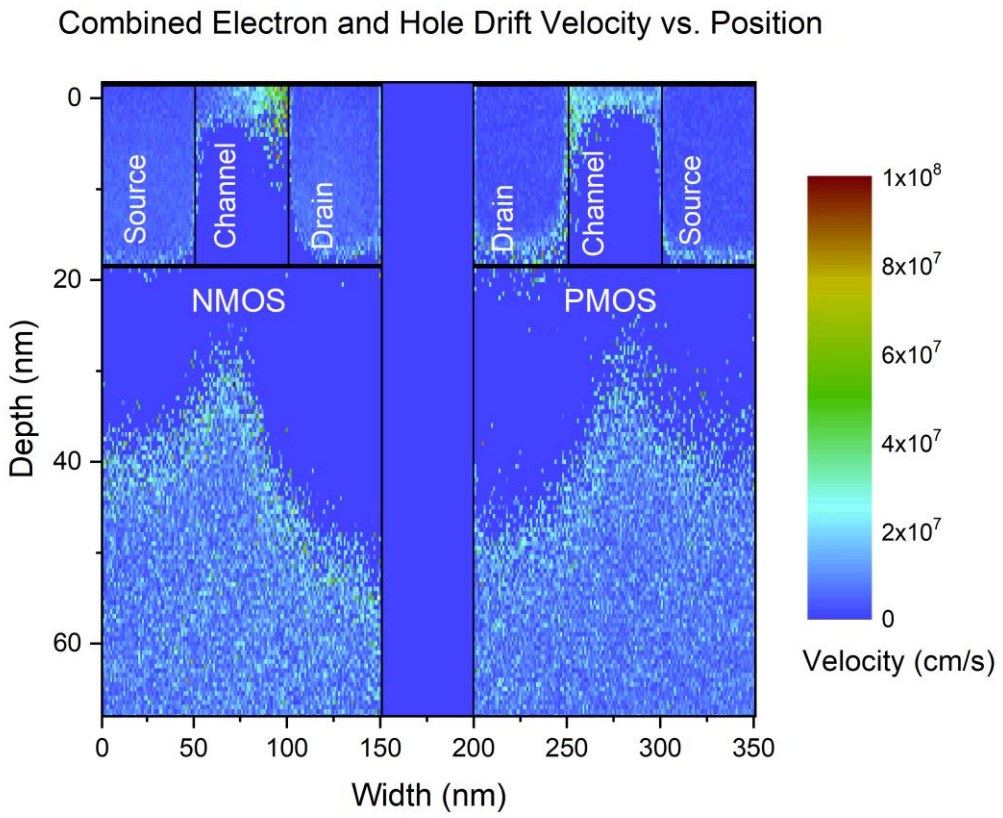

Figure 39 - Combined Drift Velocity: Velocity in the MOSFET channel regions is due to the applied bias. The resulting electric field exerts a force on the charge carriers in the inversion layer (electrons in the n-channel and holes in the p-channel). Velocity in the bulk region is dominated by random motion of carriers, but with slightly higher average velocity near the edges of the depletion region due to diffusion along the concentration gradient.

The combined electron and hole drift velocity is used to calculate the total combined drift energy, effectively combining the profiles from Fig. 34. One of the notable considerations in this calculation is that the dispersion relation differs between electrons in the conduction band and holes in the valence band, as discussed in chapter 2. The relation between drift

velocity and drift energy differs as well. The combined drift energy, shown in Fig. 40, highlights this difference.

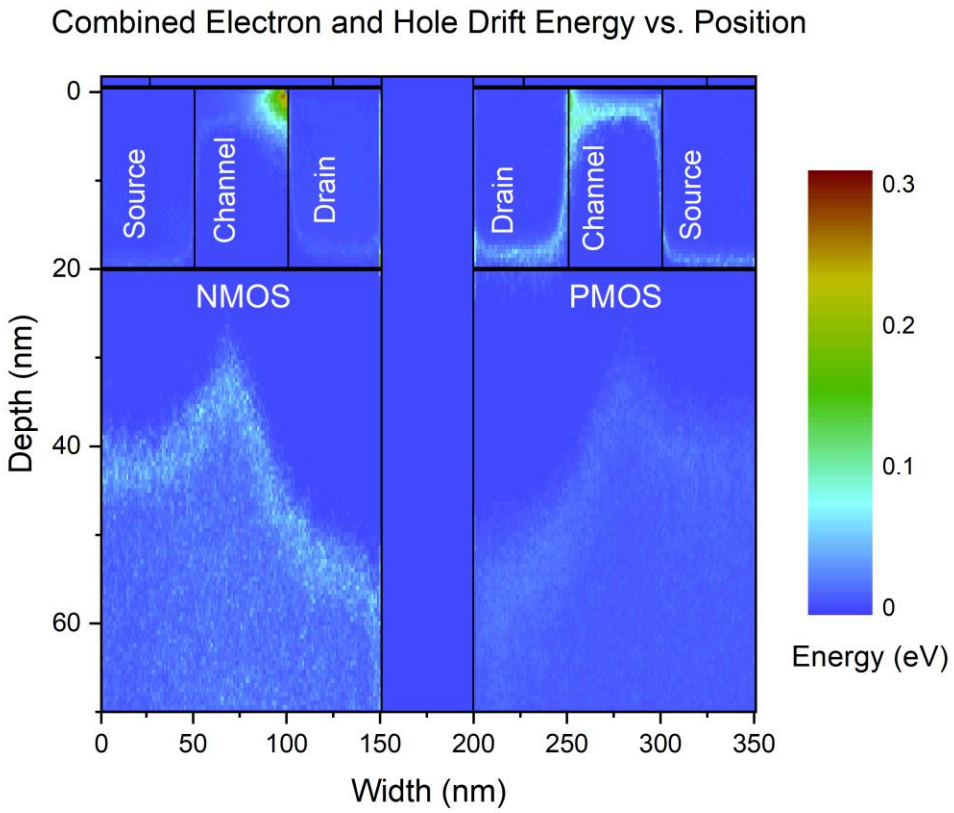

Figure 40 - Combined Drift Energy: Energy in the MOSFET channel regions is due to the applied bias. Differences in the energy profile between the n-channel and p-channel can be attributed both to the differences in electron and hole drift velocity as well as the difference in the dispersion relation for electrons and holes. Drift energy in the bulk region is primarily due to random motion of carriers; thus, differences in the energy profile in the bulk regions are attributed to differences in the dispersion relation for electrons and holes.

The Monte Carlo solver calculates thermal energy of the electrons and holes, calculating the total thermal energy profile effectively combines the profiles from Fig. 35. Differences in the thermal energy profile, shown in Fig. 41, in the NMOS and PMOS are attributed to differences in transport behavior for electrons and holes.

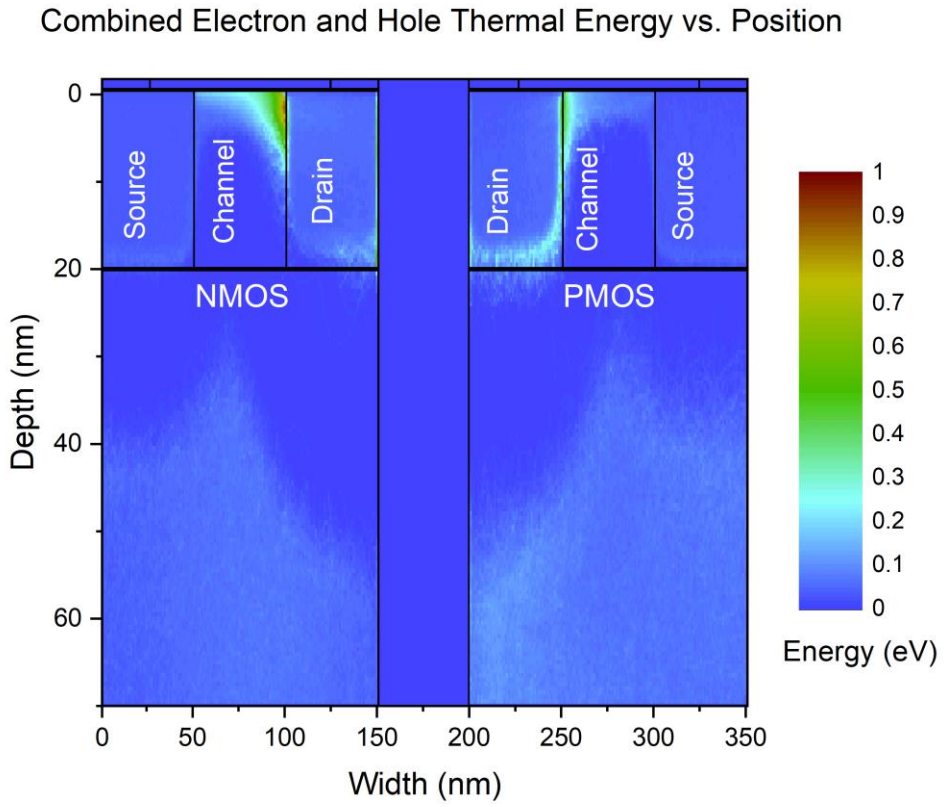

Figure 41 - Combined Thermal Energy: Energy in the MOSFET channel regions is due to the applied bias. The resulting electric field exerts a force on the charge carriers in the inversion layer (electrons in the n-channel and holes in the p-channel). Thermal energy in the bulk region for both electrons and holes exceeds the thermal energy at room temperature (3kT/2=38 meV) due to hot carrier effects in the channel that cause an increase in temperature throughout the device structure.

The combined electron and hole thermal energy is used to determine combined electron and hole temperature profile, effectively combining the profiles from Fig. 36. The difference in the carrier temperature profile, shown in Fig. 42, in the NMOS and PMOS is attributed to the difference in thermal energy of electrons and holes due to their differing charge transport behavior.

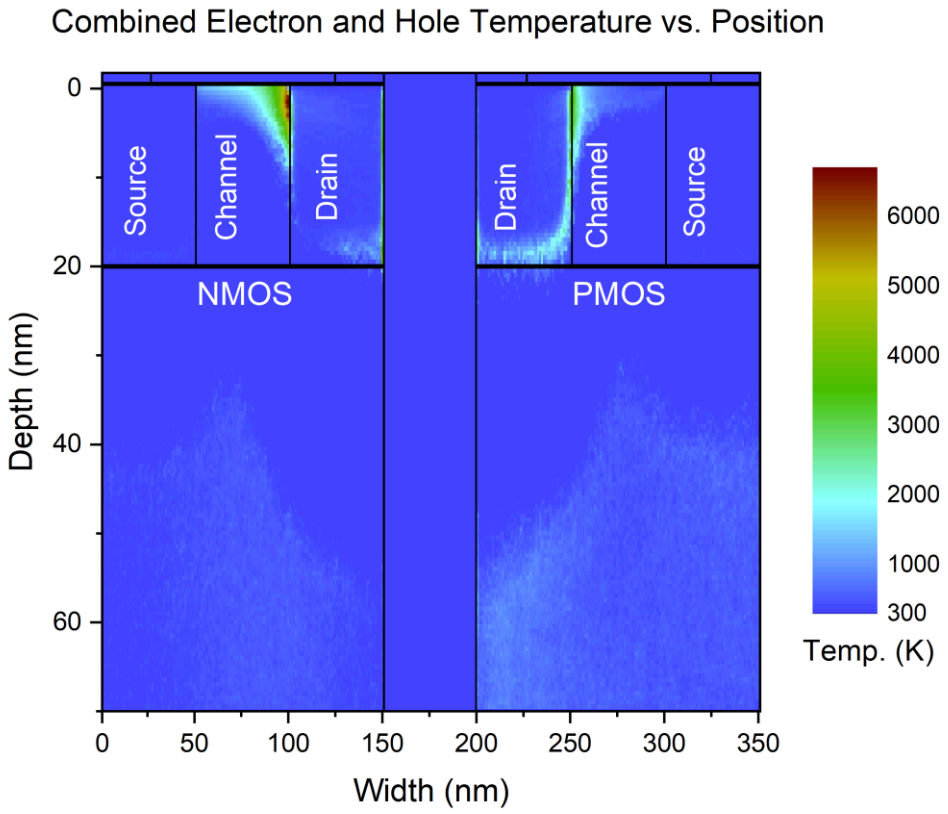

Figure 42 - Combined Carrier Temperature: Increased temperature in the MOSFET channel regions is due to the applied bias. The resulting electric field exerts a force on the charge carriers in the inversion layer (electrons in the n-channel and holes in the p-channel). Carrier temperature in the bulk region for both electrons and holes exceeds room temperature due to hot carrier effects in the channel that cause an increase in temperature throughout the device structure.

With the drift energy thermal energy of both electrons and holes the total energy is calculated, effectively combining the profiles in Fig. 37. Total energy indicates the magnitude of the contribution from hot-carriers to thermal transport. Differences in the total energy profile for NMOS and PMOS devices indicate the extent to which differences in charge transport behavior of electrons and holes affects the thermal transport in these devices. Figure 43 shows the combined total energy profile for electrons and holes.

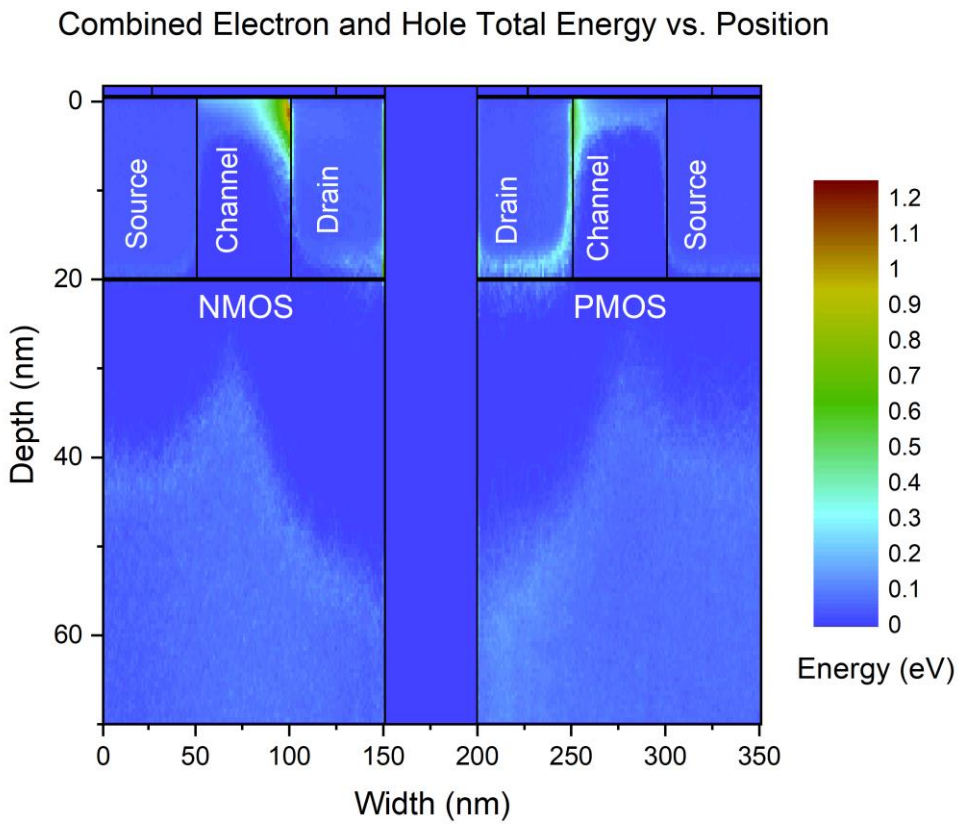

Figure 43 - Combined Total Energy: Energy in the MOSFET channel regions is due to the applied bias. The resulting electric field exerts a force on the charge carriers in the inversion layer (electrons in the n-channel and holes in the p-channel). Energy in the bulk region is dominated by random motion of the carriers and increased temperature in the device.

7.4 Device Thermal Profiles

The energy balance method of evaluating for thermal transport gives a thermal profile in the device which accounts for hot carrier effects of both electrons and holes. One important assumption in the derivation of Eq. (7.6) is equating the lattice temperature and the acoustic phonon temperature. With this assumption, the acoustic phonon temperature profile gives the temperature profile of the device crystal lattice as well. The optical phonon temperature profile in Fig. 44 shows localized hot spots forming due to hot-carrier effects in the NMOS and PMOS channel regions. The lattice temperature profile in Fig. 45 shows how the

thermal energy generated in these hot spots spreads out and causes an increase in temperature throughout the structure.

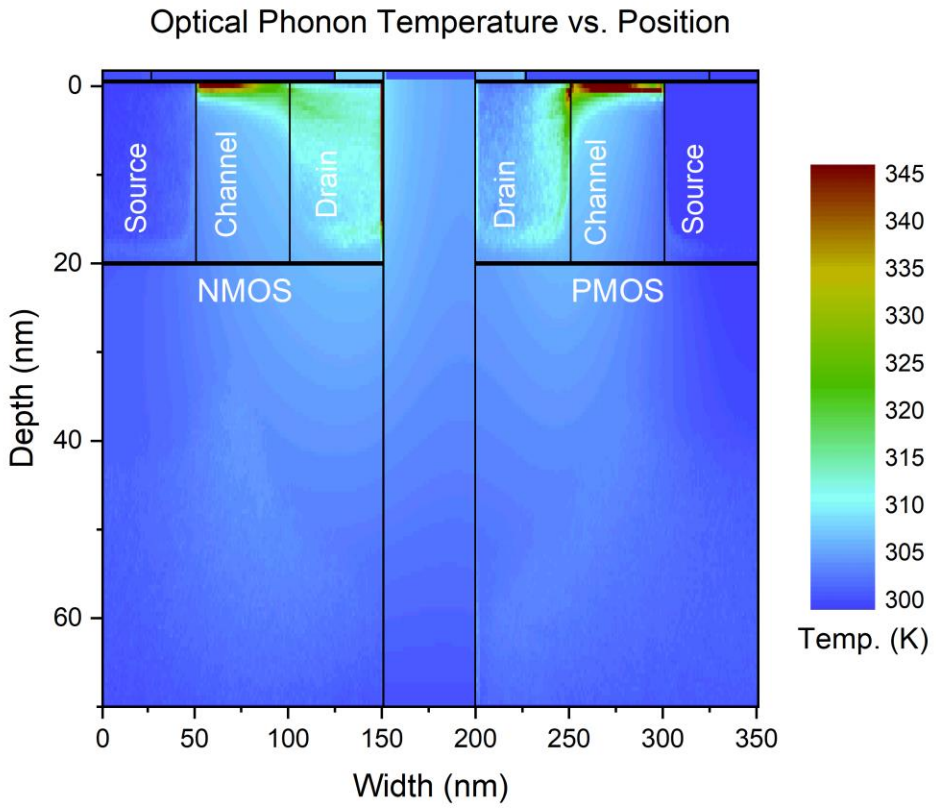

Figure 44 - Optical Phonon Temperature: The optical phonon temperature profile reveals the shape and location of the hot spots that form from hot carrier effects in the NMOS and PMOS channel regions.

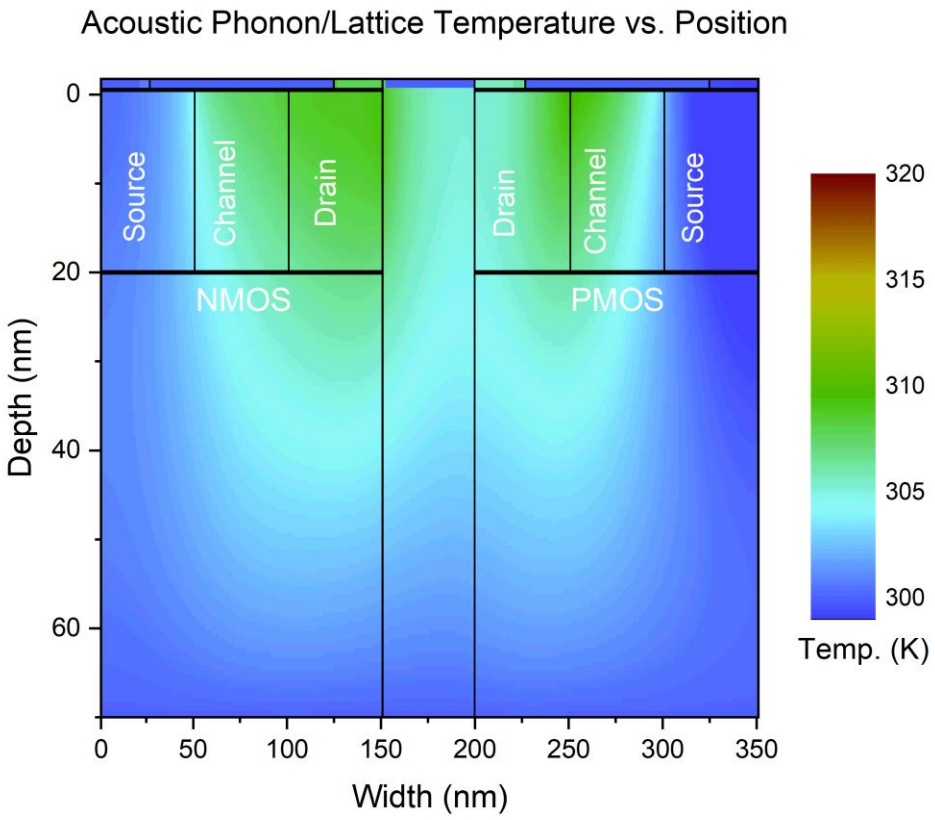

Figure 45 - Acoustic Phonon/Lattice Temperature: While the optical phonon temperature profile shows the hot spot, the lattice temperature profile reveals how this hot spot results in increased temperature throughout the structure.

CHAPTER 8

CONCLUSIONS

The Monte Carlo method of modeling charge transport has a long history of use in the computational study of semiconductor microelectronic devices. It is versatile, accurate, and provides a level of detail with regards to the behavior of individual charged particles that far exceeds continuum-based alternatives. Many studies in the literature include only a single conductivity type. Electron Monte Carlo simulations are used to study bulk properties in n-type materials and devices with electrons as majority or inversion layer carriers. Hole Monte Carlo simulations are used to study bulk properties in p-type materials and devices with holes as majority or inversion layer carriers. This dissertation demonstrates that combining electrons and holes in the Monte Carlo ensemble allows for the study of NMOS and PMOS devices concurrently using the same solver.

Heat transfer studies in computational electronics is increasingly important subject as dimensional scaling precipitates an increase in current density in semiconductor devices. Traditionally, the favored approach is to use the Joule's heating law in conjunction with Fourier's law to model the effects of resistive heating in electronic devices. The differential form of Joule's heating law relates the power per unit volume of heat dissipation with the current density and electric field; thus, the use of the Joule heating model to determine generation terms in the heat transfer equation is often called the J·E method. This dependence on current density and electric field makes this method an intuitive choice for modeling of electronic devices, since these are fundamental characteristics of interest when evaluating device behavior. These quantities are available or calculable in the preferred charge transport modeling schemes.

The Joule heating method of studying heat transfer in semiconductor electronics becomes ineffective for sufficiently small devices, since dimensional scaling also precipitates an increase in electric field strength in critical device regions. High electric fields result in hot-carrier effects playing a role in both charge transport as well as thermal transport. In the realm of charge transport, the thermal energy of excited carriers increases their scattering rates as they move around the device; however, the increase is not enough to prevent other high field effects like velocity overshoot and ballistic transport. Some of these effects can be incorporated into continuum methods using modified mobility models, whereas some require a transition to a stochastic approach such as the Monte Carlo method. In the realm of thermal transport, hot-carrier effects result in local thermal non-equilibrium; the thermal energy of an excited charge carrier exceeds that of its surroundings. This thermal non-equilibrium is incompatible with continuum models which describe the thermal energy in a system in terms of a simple temperature profile.

The energy balance approach allows for thermal non-equilibrium by separately evaluating the thermal energy of charge carriers, optical phonons, and acoustic phonons. Previously, this method was successfully implemented in semiconductor device electro-thermal simulations and coupled with multiscale thermal transport simulations at the circuit level. These previous successes used the Monte Carlo method for charge transport and the energy balance method for thermal transport while only considering the contributions from electrons. This dissertation shows that the electro-thermal methodology is also effective when considering the contributions of both electrons and holes.

Future work may couple the dual carrier electron-thermal modeling approach with a multiscale approach for simulating thermal transport at the circuit level. It may become

possible to simulate entire CMOS circuits with the accuracy and precision of device level simulations.

REFERENCES

[1] A. S. Sedra, *Microelectronic circuits*, 6th ed. New York, NY: Oxford University Press, 2010.

[2] P. Horowitz, *The art of electronics*, 2nd ed. Cambridge, MA: Cambridge University Press, 1980.

[3] G. Hiblot, "DIBL-Compensated Extraction of the Channel Length Modulation Coefficient in MOSFETs," *IEEE Trans. Electron Devices*, vol. 65, no. 9, pp. 4015–4018, 2018.

[4] D. Vasileska and S. M. Goodnick, *Computational electronics*. San Rafael, CA: Morgan & Clapool Publishers, 2006.

[5] M. Pourfath, V. Sverdlov, and S. Selberherr, "Transport modeling for nanoscale semiconductor devices," *Solid-State and Integrated Circuit Technology (ICSICT), 2010 10th IEEE International Conference on*. pp. 1737–1740, 2010.

[6] V. Sverdlov, E. Ungersboeck, H. Kosina, and S. Selberherr, "Current transport models for nanoscale semiconductor devices," *Mater. Sci. Eng. R*, vol. 58, no. 6, pp. 228–270, 2008.

[7] E. Pop, S. Sinha, and K. E. Goodson, "Heat Generation and Transport in Nanometer-Scale Transistors," *Proc. IEEE*, vol. 94, no. 8, pp. 1587–1601, 2006.

[8] S. Gaur and D. Navon, "Two-dimensional carrier flow in a transistor structure under nonisothermal conditions," *IEEE Trans. Electron Devices*, vol. 23, no. 1, pp. 50–57, 1976.

[9] G. Wachutka, "Rigorous thermodynamic treatment of heat generation and conduction in semiconductor device modeling," *IEEE Trans. Comput. Des. Integr. Circuits Syst.*, vol. 9, no. 11, pp. 1141–1149, 1990.

[10] S. J. Kim, T.H. Shim, K. R. Choi, and J. G. Park, "Comparative study of self-heating effect on electron mobility in nano-scale strained silicon-on-insulator and strained silicon grown on relaxed sige-on-insulator n-metaloxidesemiconductor field-effect transistors," *Semicond. Sci. Technol.*, vol. 24, no. 3, p. 35014, 2009.

[11] A. Majumdar, K. Fushinobu, and K. Hijikata, "Effect of gate voltage on hot-electron and hot phonon interaction and transport in a submicrometer transistor," *J. Appl. Phys.*, vol. 77, no. 12, pp. 6686–6694, 1995.

[12] A. Raman, D. Walker, and T. Fisher, “Simulation of nonequilibrium thermal effects in power LDMOS transistors,” *Solid State Electron.*, vol. 47, no. 8, pp. 1265–1273, 2003.

[13] K. Raleva, D. Vasileska, S. M. Goodnick, and M. Nedjalkov, “Modeling Thermal Effects in Nanodevices,” *Electron Devices, IEEE Trans.*, vol. 55, no. 6, pp. 1306–1316, 2008.

[14] J. Lai and A. Majumdar, “Concurrent thermal and electrical modeling of sub-micrometer silicon devices,” *J. Appl. Phys.*, vol. 79, no. 9, pp. 7353–7361, 1996.

[15] A. Akkerman, M. Murat, and J. Barak, “Monte Carlo calculations of electron transport in silicon and related effects for energies of 0.02-200 keV,” *J. Appl. Phys.*, vol. 106, no. 11, 2009.

[16] B. D. Tierney, “Monte Carlo Studies of Electron Transport in Semiconductor Nanostructures,” Ph.D. Dissertation, Dept. Elect. Eng., Arizona State Univ., Tempe, AZ, 2011.

[17] J. Dewey and M. A. Osman, “Monte Carlo study of hole transport in silicon,” *J. Appl. Phys.*, vol. 74, no. 5, pp. 3219–3223, 1993.

[18] S. Jallepalli, M. Rashed, W. K. Shih, C. M. Maziar, and A. F. Tasch, “A full-band Monte Carlo model for hole transport in silicon,” *J. Appl. Phys.*, vol. 81, no. 5, pp. 2250–2255, 1997.

[19] M. Cohen and T. Bergstresser, “Band Structures and Pseudopotential Form Factors for Fourteen of the Diamond and Zinc-blende Structures,” *Phys. Rev.*144, pp. 789, 1966.

[20] J. M. Hinckley and J. Singh, “Monte Carlo studies of ohmic hole mobility in silicon and germanium: Examination of the optical phonon deformation potential,” *J. Appl. Phys.*, vol. 76, no. 7, pp. 4192–4200, 1994.

[21] T. Sadi, R. Kelsall, and N. Pilgrim, “Electrothermal Monte Carlo simulation of submicrometer Si/SiGe MODFETs,” *IEEE Trans. Electron Devices*, vol. 54, no. 2, pp. 332–339, 2007.

[22] D. Vasileska, “Modeling thermal effects in nano-devices,” *Microelectron. Eng.*, vol. 109, pp. 163–167, 2013.

[23] S. S. Qazi, “Electrical and Thermal Transport in Alternative Device Technologies,” M.S. Thesis, Elect. Eng., Arizona State Univ., Tempe, AZ, 2013.

[24] A. Hossain, D. Vasileska, and S. M. Goodnick, “Self-heating and short-range Coulomb interactions due to traps in a 10 nm channel length nanowire transistor,” in *2011 11th IEEE International Conference on Nanotechnology*, pp. 1110–1113, 2011.

[25] M. Artaki and P. J. Price, “Hot phonon effects in silicon field-effect transistors,” *J. Appl. Phys.*, vol. 65, no. 3, pp. 1317–1320, 1989.

[26] E. Ramayya, “Thermoelectric properties of ultrascaled silicon nanowires,” Ph.D. dissertation, Elect. Eng., Univ. Wisconsin-Madison, Madison, WI, 2010.

[27] A. R. Shaik, D. “Multi Scale Study of Heat Transfer Using Monte Carlo Technique for Phonon Transport,” M.S. Thesis, Dept. Elect. Eng., Arizona State Univ., Tempe, AZ, 2016.

[28] E. Pop, R. W. Dutton, and K. E. Goodson, “Analytic band Monte Carlo model for electron transport in Si including acoustic and optical phonon dispersion,” *J. Appl. Phys.*, vol. 96, no. 9, pp. 4998–5005, 2004.

[29] A. Abramo *et al.*, “A Multiband Model for Hole Transport in Silicon at High Energies,” *Semicond. Sci. Technol.*, vol. 7, no. 3B, pp. B597–B600, 1992.

[30] J. R. Nagel, “Numerical Solutions to Poisson Equations Using the Finite-Difference Method,” *Antennas Propag. Mag. IEEE*, vol. 56, no. 4, pp. 209–224, 2014.

[31] S. E. Laux, “On particle-mesh coupling in Monte Carlo semiconductor device simulation,” *Comput. Des. Integr. Circuits Syst. IEEE Trans.*, vol. 15, no. 10, pp. 1266–1277, 1996.

[32] Z. Aksamija, H. S. Hahm, and U. Ravaioli, “Emission and absorption of phonons in silicon,” *Phys. status solidi*, vol. 5, no. 1, pp. 90–93, 2008.

[33] K. Raleva, E. Bury, B. Kaczer, and D. Vasileska, “Uncovering the temperature of the hotspot in nanoscale devices,” in *2014 International Workshop on Computational Electronics (IWCE)*, pp. 1–3, 2014.